MAXIMUM SCOUR AROUND CYLINDERS INDUCED BY WAVE AND CURRENT ACTION

by

ABUBAKER MOHAMED ABUSBEAA

A THESIS SUBMITTED IN PARTIAL FULFILMENT OF

THE REQUIREMENTS FOR THE DEGREE OF

MASTER OF APPLIED SCIENCE

in

FACULTY OF GRADUATE STUDIES

Department of Civil Engineering

We accept this thesis as conforming

to the required standard

THE UNIVERSITY OF BRITISH COLUMBIA

JUNE, 1986

© ABUBAKER MOHAMED ABUSBEAA, 1986

In presenting this thesis in partial fulfilment of the requirements for an advanced degree at the University of British Columbia, I agree that the Library shall make it freely available for reference and study. I further agree that permission for extensive copying of this thesis for scholarly purposes may be granted by the head of my department or by his or her representatives. It is understood that copying or publication of this thesis for financial gain shall not be allowed without my written permission.

Department of Civil Engineering

The University of British Columbia
1956 Main Mall
Vancouver, Canada
V6T 1Y3

Date June, 1986

DE-6 (3/81)

ABSTRACT

The maximum possible scour around cylindrical structures under the action of combined wave and current was investigated in this study. A review of the literature showed that there are no adequate theories or methods for predicting maximum possible scour depths around structures under the action of wave plus current. Development of such a scour prediction is of considerable economic importance for the design of offshore structures. The study started with experimental tests of the scour around cylindrical structures and a comparison was made between scour under steady currents alone, waves alone and combined wave and current conditions. Existing theories for scour and flow velocities under waves alone and currents alone were analyzed and sets of experiments were performed for the three flow conditions of waves alone, currents and waves plus currents using three sediment size ranges and five cylinder sizes. The dependence of maximum scour on both cylinder size and sediment size for the three flow cases was studied and graphical relationships were established. The maximum scour under combined wave and current at threshold conditions in the approaching flow was investigated in detail and the dependence of maximum scour on this critical threshold flow criterion was shown. The maximum scour depth can be roughly estimated using this study provided that the flow conditions, sediment properties and structure dimensions are defined.

TABLE OF CONTENTS

TABLE OF CONTENTS (Continued)

LIST OF TABLES

LIST OF FIGURES

LIST OF FIGURES (Continued)

LIST OF FIGURES (Continued)

NOMENCLATURE

a = maximum dimension of the particle

a_{1m} = amplitude of horizontal particle motion in the oscillatory flow

A = projected area of object normal to flow direction

b_o = intermediate dimension of the particle

b = cylinder diameter

c = minimum dimension of the particle

C_a = wave celerity relatrive to the fixed coordinate system

C_1 = form coefficient

C_2 = form coefficient related to the effective surface area of the particle in the direction of the drag force

C_3 = form coefficient related to the effective surface area of the particle in the direction of the lift force

C_D = drag coefficient

C_L = lift coefficient

C_r = wave celerity relative to the coordinate from moving with current

d, d_o = water depth in the channel

d_{sm} = maximum scour depth

d_{se} = equilibrium scour depth

d_n = diameter of a sphere having the same volume as the particle

d_A = diameter of a sphere having the same surface area as the particle

D = mean particle size of bed roughness elements

D_s = characteristic diameter of the particle

f_c = friction factor for unidirectional flow

f_w = friction factor for oscillatory flow

f_{wc} = friction factor for combined wave and current

F_D = drag force

F_g = gravity force

F_L = lift force

F_p = pile Froude number

F_r = Froude number

F_T = total force

F_s^* = entrainment function

g = gravitational constant

H = wave height

H_R = height of reflected wave

H_{max}, H_{min} = maximum and minimum wave heights measured in the flume

k = wave number = $2\pi/L$

k_s = height of bed roughness element

K_c = Keulegan-Carpenter number $U_{lm}T/b$

K_r = reflection coefficient for flume waves = H_R/H

n = Manning's roughness coefficient

P_a = Pascal

R_e = Reynold's number

R_e^* = particle Reynold's number = U^*D/ν

R_p = pile Reynold's number = Ub/ν

R_h = hydraulic radius of channel

S_s = specific gravity of particles

S_o = channel bed slope

S = maximum scour depth

S_F = shape factor

T = wave period

T_a = period of wave on current as seen from moving coordinate frame

U = flow velocity

U_{1m} = maximum orbital velocity at the bed as predicted by first order theory

U_c = steady current average velocity

U_{cr} = flow critical velocity

U_w = maximum oscillatory water particle velocity

U^* = friction velocity = $(\tau/\rho)^{1/2}$

U^*_{cr} = friction velocity at threshold conditions

U^*_{wc} = equivalent shear velocity for combined wave and current flow

v = fall velocity

α = constant

γ = specific weight of fluid

γ_s = specific weight of sediment

μ = dynamic viscosity

ν = kinematic viscosity = μ/ρ

ρ = fluid density

ρ_s = sediment density

τ = shear stress

τ_o = shear stress at bed

τ_c = steady current shear stress

τ_{cr} = critical shear stress

τ_w = unsteady flow shear stress

τ_{wc} = combined wave and current shear stress

ϕ = angle of repose of the submerged sediment

ϕ_c = angle made by unidirectional current with the direction of wave propagation

ACKNOWLEDGEMENTS

The author is very grateful for the guidance and encouragement given by his supervisor, Dr. M.C. Quick throughout the preparation of this thesis.

Financial support in the form of a scholarship from Al-Fatch University, Tripoli is gratefully acknowledged.

The author wishes to thank Mr. Kurt Nielsen for his technical expertise and invaluable support in the laboratory.

The author is thankful for the encouragement and advice by his fellow graduate students.

1. INTRODUCTION

1.1 GENERAL

In the accelerated exploration of offshore resources there is a growing need to place objects or structures on the sea bed. Design considerations must include an analysis of their stability, particularly if the sea bed is composed of non-cohesive sediments. A sand-bottom material is generally in a condition of dynamic stability under the prevailing currents and wave-induced currents. When an object is placed in or on the sea-bed, the equilibrium may be disturbed and local velocities around the objects are increased and the rate of transported material is increased. This increase in the transported material may cause scouring (erosion) around the structures.

Current and wave conditions in the vicinity of the structure will change. This change may cause large changes in the bottom topography in the vicinity of the structure and thus cause erosion in some and deposition in other areas. The depth of scour around structures is important in computing the minimum penetration depth of piles for fixed structures. For objects placed on the bottom, or for "sit-on-bottom" platforms the scour may cause settlement of the supporting members.

The main purpose of this investigation is to develop predictions of scour depth around offshore structures under the combined action of currents and waves. Scour depth experiments for cylindrical piles were conducted in this study and comparison was made between the scour produced by currents alone, waves alone and waves plus currents. The study will be restricted to determining scour depths around cylindrical

structures placed in non-cohesive granular bed material and with flows in the direction of wave propagation. The main emphasis will be concerned with estimating the maximum possible scour.

1.2 LITERATURE REVIEW

1.2.1 SCOUR

Many types of scour exist, for example general scour, where bed level degrades because sediment removal exceeds sediment supply, local scour where the bed level locally drops, usually caused by local acceleration of the flow around a structure. These types are sub-divided into live bed and clear water scour. Live bed scour occurs where sediment supply equals sediment removal while clear water scour occurs when there is no sediment supply.

In general, clear water scour depths are greater than general scour depths as pointed out by many investigators, e.g. Melville (1975) and Jain and Fisher (1980), hence only clear water scour case will be dealt with in this study. The scour due to steady currents alone, waves alone, and combined current plus waves is discussed in the following section.

1.2.2 UNIDIRECTIONAL FLOWS - STEADY CURRENTS - SCOUR

Scour around cylindrical piles has long been of importance in the design of bridge piers and ocean jetties for more than a century and it has been the subject of many investigations such as Anderson (1974), Breusers et al. (1977). Jain and Fisher (1979), Neill (1964a) and Shen et al. (1966). Numerous scour predictions formulas have been published as a result of these studies, but predicted scour depths vary widely,

especially when the formulas are applied to flow conditions outside the range of conditions for which they were developed. However in spite of the variations, there does appear to be consensus. Once the conditions of general sediment motion have been established in a stream, there will be no further increase in scour depth with velocity, because the rate at which sediment enters the region of scour is equal to the rate of removal by the scouring process.

Few investigations have been made for flows at higher velocities, i.e., for flow regimes well beyond the onset of general sediment transport. This limited number of investigations is because performing experiments at high velocities beyond the onset of motion (Threshold velocity) needs a continuous supply or recirculation of sediment material which is a difficult process.

Water flowing past a structure founded on an erodible sediment bed is frequently observed to produce local scouring. This scouring results from the acceleration and deceleration of the water flow field as it flows past the structure and these are the regions of local erosion and deposition of sediment.

The dominant features of the flow near a pier is the large-scale eddy structure, or the system of vortices which develop around the pier. These vortex systems are the basic mechanism of local scour, which has long been recognized by many investigators including Melville (1975), Neill (1964b), Roper (1967), Imberger et al. (1982). Due to the placing of an obstruction in the flow field, locally high velocities are produced around the pier which increase the tractive force on the sediment at the pier base. Due to the non-uniform velocity distribution in a stream flow, the pressure field induced by the pier: (1) creates a downward

velocity along the lower leading face of the pier; and (2) produces a three-dimensional separation of the boundary layer leading to the formation of a horseshoe vortex. According to Melville (1975), once the process has begun, it is the downward flow impinging on the bed, and the horseshoe vortex transporting dislodged particles away which causes the scour. In the case of clear water scour as the scour depth increases, the strength of the downward flow decreases near the bottom until finally, it can no longer dislodge particles. This condition represents the maximum scour to be attained by the prevailing flow conditions.

Experimental observations by Roper et al. (1967) show that the side slopes of the scour hole in the clear water regime are approximately equal to the natural angle of repose of the bed material. This indicates that the scour mechanism is in the immediate vicinity of the structure base, and the sediment slides in towards the base before it is removed. In the case in which there is a net sediment transport in the stream, the strength of the flow near the bottom similarly decreases with increasing scour depth, but maximum scour is attained when the rate of sediment removal is equal to the rate of sediment transported into the scour hole by the stream. The visual observation of the scour process in the general scour regime at high flow velocities show that a dynamic equilibrium exists between scour hole and stream flow which is not apparent when the flow is stopped, the flow field near the base of the pier is strong enough to support the sides of the scour hole at angles greater than the angle of repose of the sediment. The sides of the scour hole periodically collapse and dump sediment into the hole, either as a dune encroaches upon the pier, or as the fluid forces supporting these sides become unstable, see Jain and Fisher (1980).

In terms of stream velocity, the maximum scour depth around a pier increases with increasing velocity until incipient sediment conditions in the stream are reached, Figure 1.1.

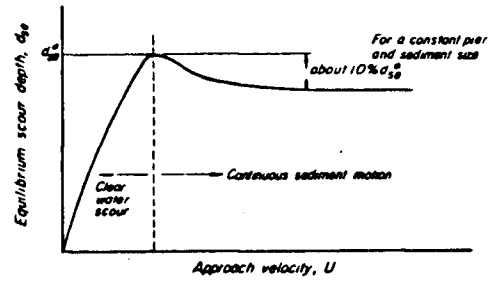

Figure 1.1 Typical scour-velocity relationship, Shen et al. (1969).

Experimental observations by Imberger et al. (1982) and Jain and Fisher (1980), then show that as the stream velocity is further increased, scour depth no longer increases but, in fact, decreases slightly, because the approaching flow is now producing a sediment discharge into the scour hole. It should be clear that the definition of onset of motion is not unique for all the studies.

Some experimental results are presented by Shen et al. (1969) as shown in Figures 1.1 through 1.4. These tests employed a steady current. Figure 1.1 shows the general trend of scour for a given pile diameter and sediment size. The 10% reduction in scour depth resulted from upstream local supply to the scour hole. Figure 1.2 indicates the scour depth as a function of the Reynold's number. Figures 1.3 and 1.4 imply that the scour depth also depends on pile diameter and sediment size.

Many formulas are available in the literature for scour depth prediction in case of unidirectional flow such as those given by Roper et al. (1967), Imberger et al. (1982) and Breusers et al. (1977). An

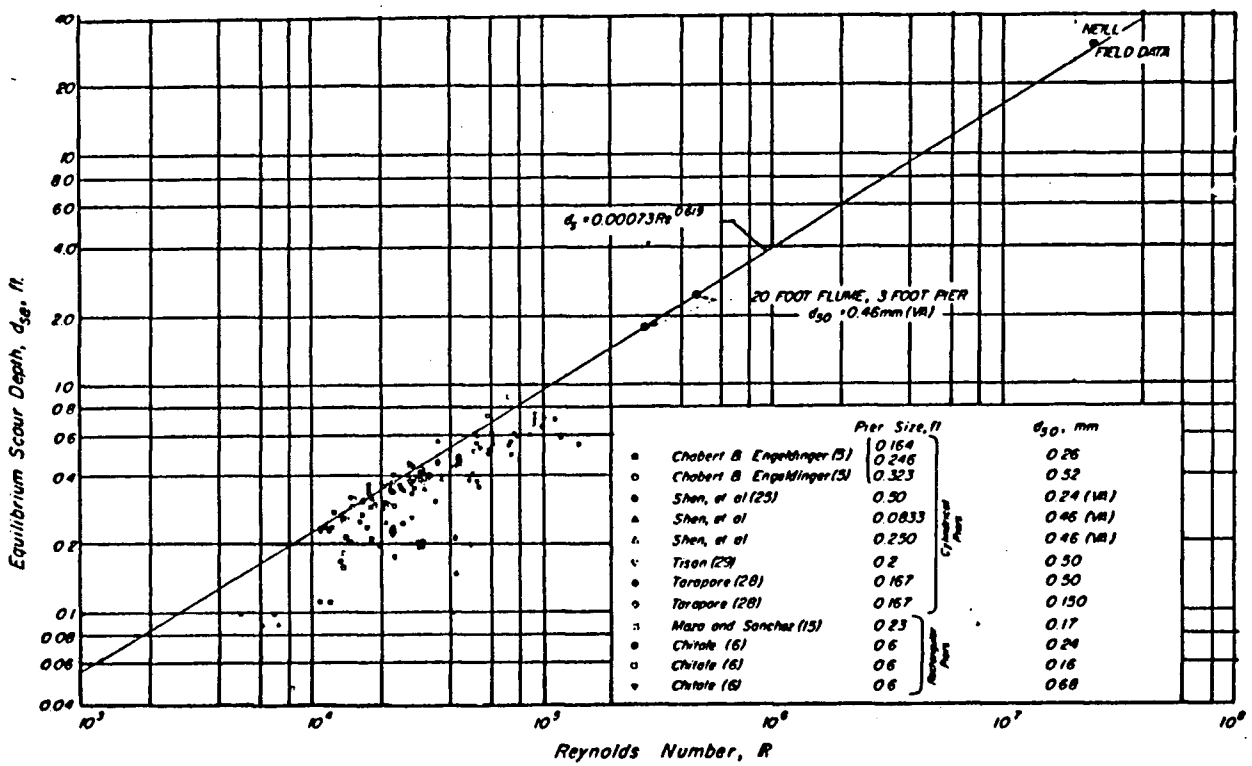

Figure 1.2 Graph of scour versus Pier Reynold's number, Shen et al. (1969).

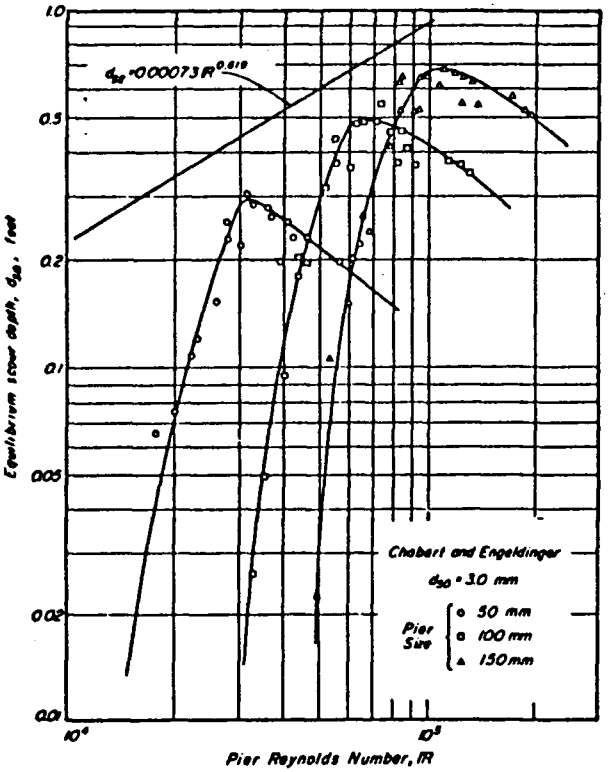

Figure 1.3 Graph of scour versus Pier Reynold's number for three different pile sizes, Shen et al. (1969).

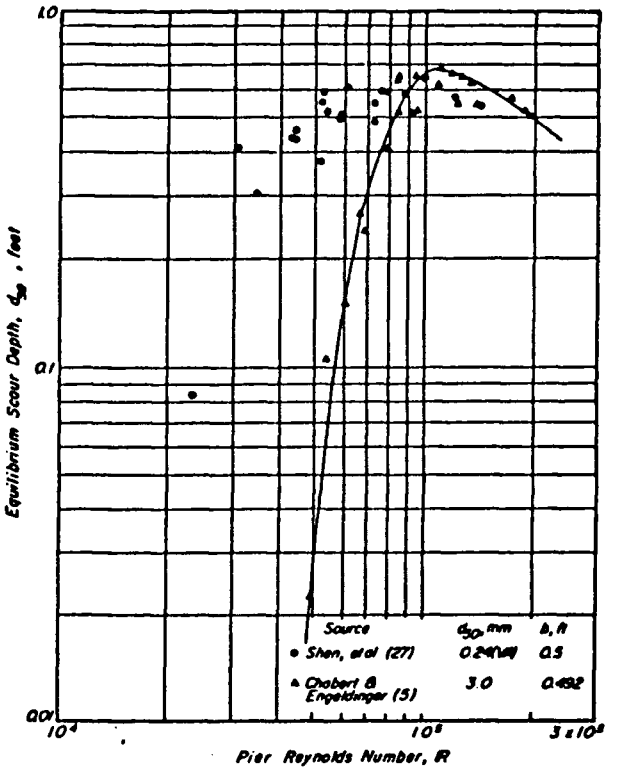

Figure 1.4 Graph of scour versus Pier Reynold's number for two different sand sizes, Shen et al. (1969).

extensive review of local scour around bridge piers is given by Breusers et al. (1977).

1.2.3 OSCILLATING FLOW - WAVES - SCOUR

Very little experimental work has been done on scour due to oscillating wave conditions, whereas there exists a wealth of knowledge on scour in open channel flow. Since the forces that cause scour virtually are the same for oscillating flow as for open channel (steady state) flow, that is, hydrodynamic in nature, the knowledge gained from experiments in open channel flow was applied, with certain reservations, by some investigators to oscillatory motion. The majority of the work done on scour in oscillatory motions has been concerned primarily with scour of beaches and littoral sediment transport.

Ko (1967), Marphy (1964), and Van Wells (1965) studied scour in front of sea walls of various angles, and their results are summarized by Herbich et al. (1965). A study of the scour due to oscillatory wave motion was conducted by Wells and Sorensen (1980). Figures 1.5 through 1.8 are graphs which resulted from their investigation. Figure 1.5 shows a definite relationship between the relative scour and the relative depth for various sediments. Figures 1.5 and 1.6 show an increasing scour depth with an increasing wave period. Figures 1.7 and 1.8 show the relative scour as a function of sediment number, and pier Reynold's number respectively.

1.2.4 COMBINED WAVES AND CURRENTS FLOW SCOUR

Scour due to waves and currents around offshore facilities is becoming an ever-increasing problem as the marine construction industry

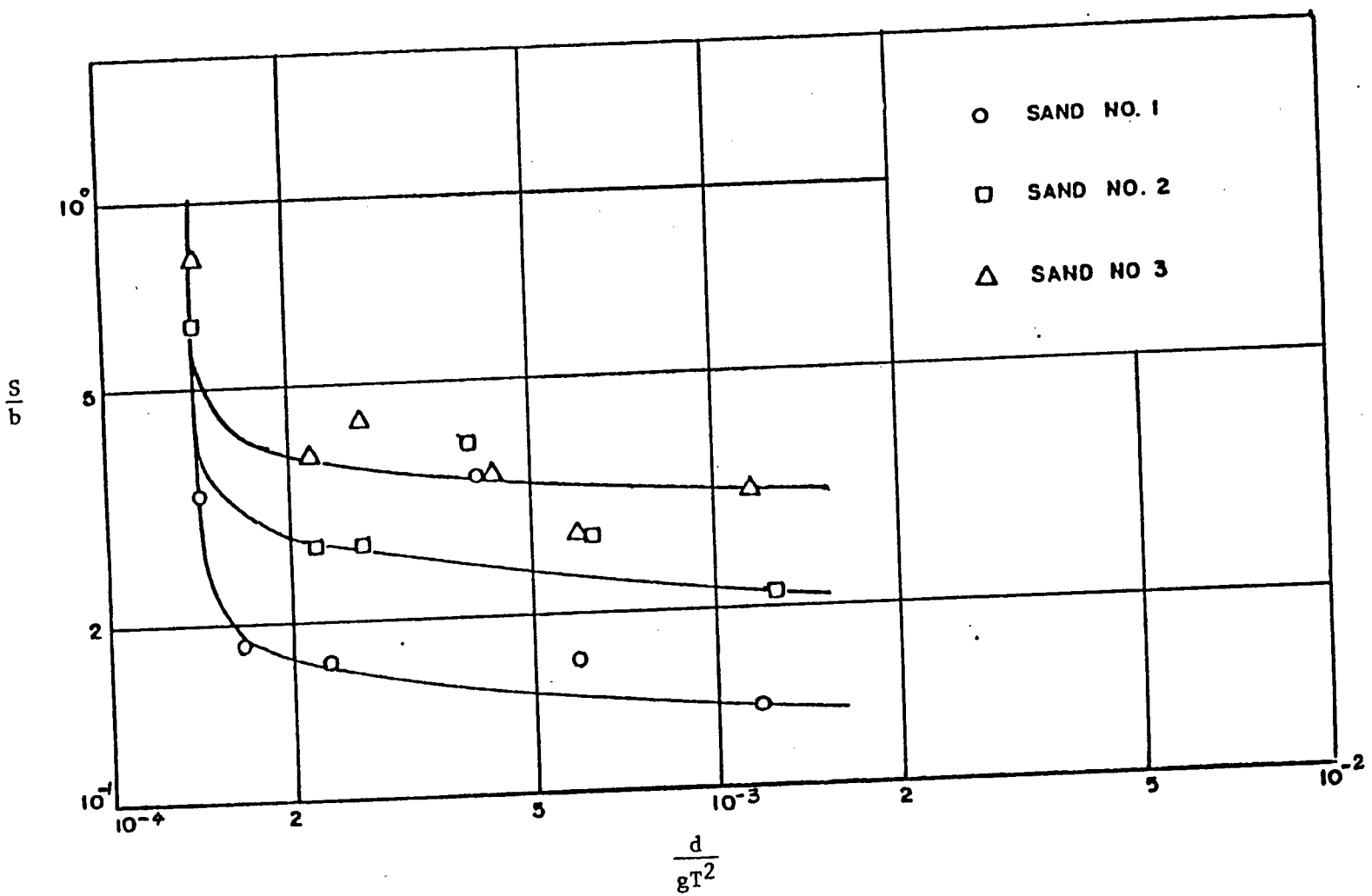

Figure 1.5. Relative scour versus relative depth, Wells and Sorensen (1970).

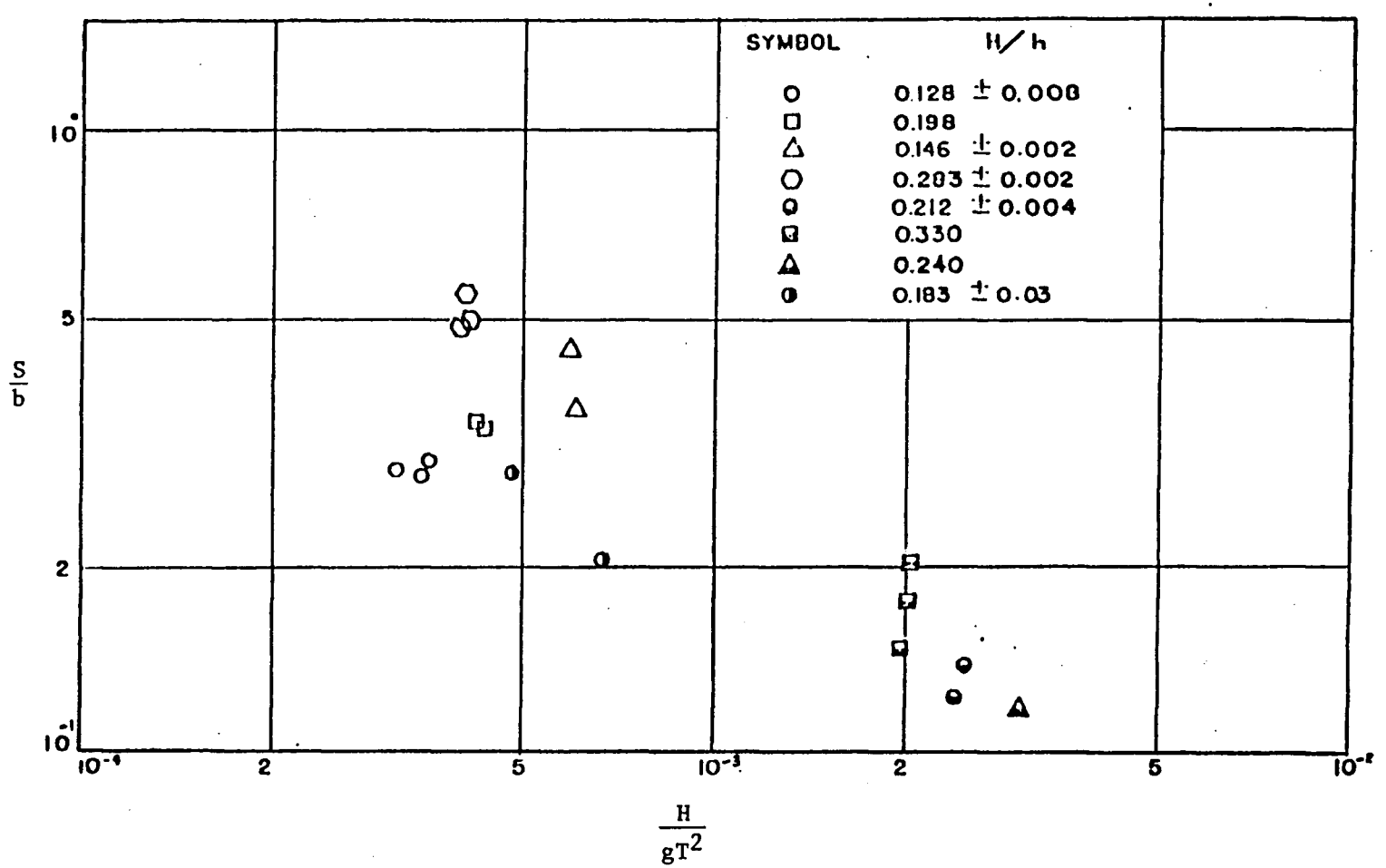

Figure 1.6. Relative scour versus wave steepness, Wells and Sorensen (1970).

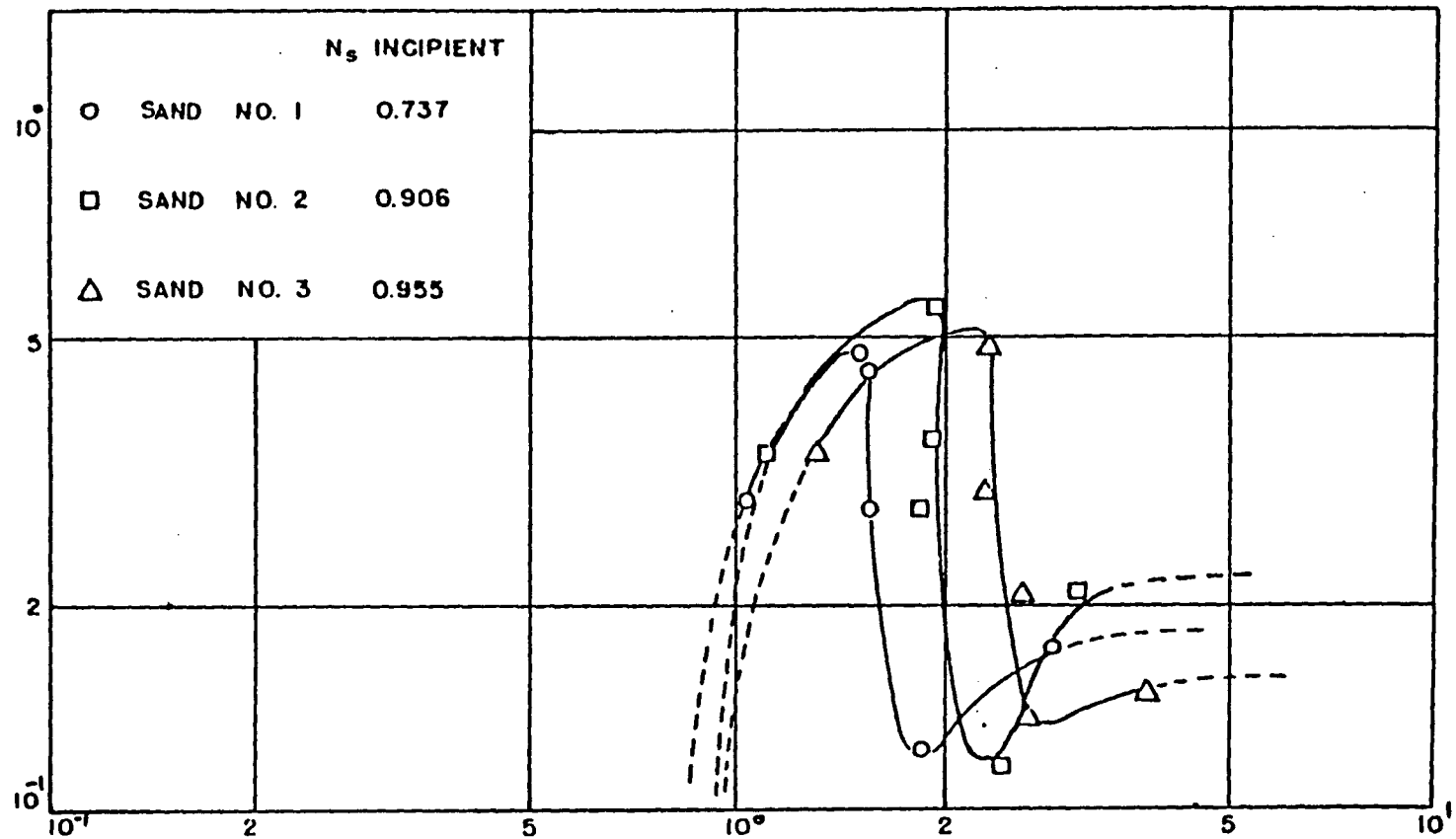

Figure 1.7. Relative scour versus sediment number, Wells and Sorensen (1970).

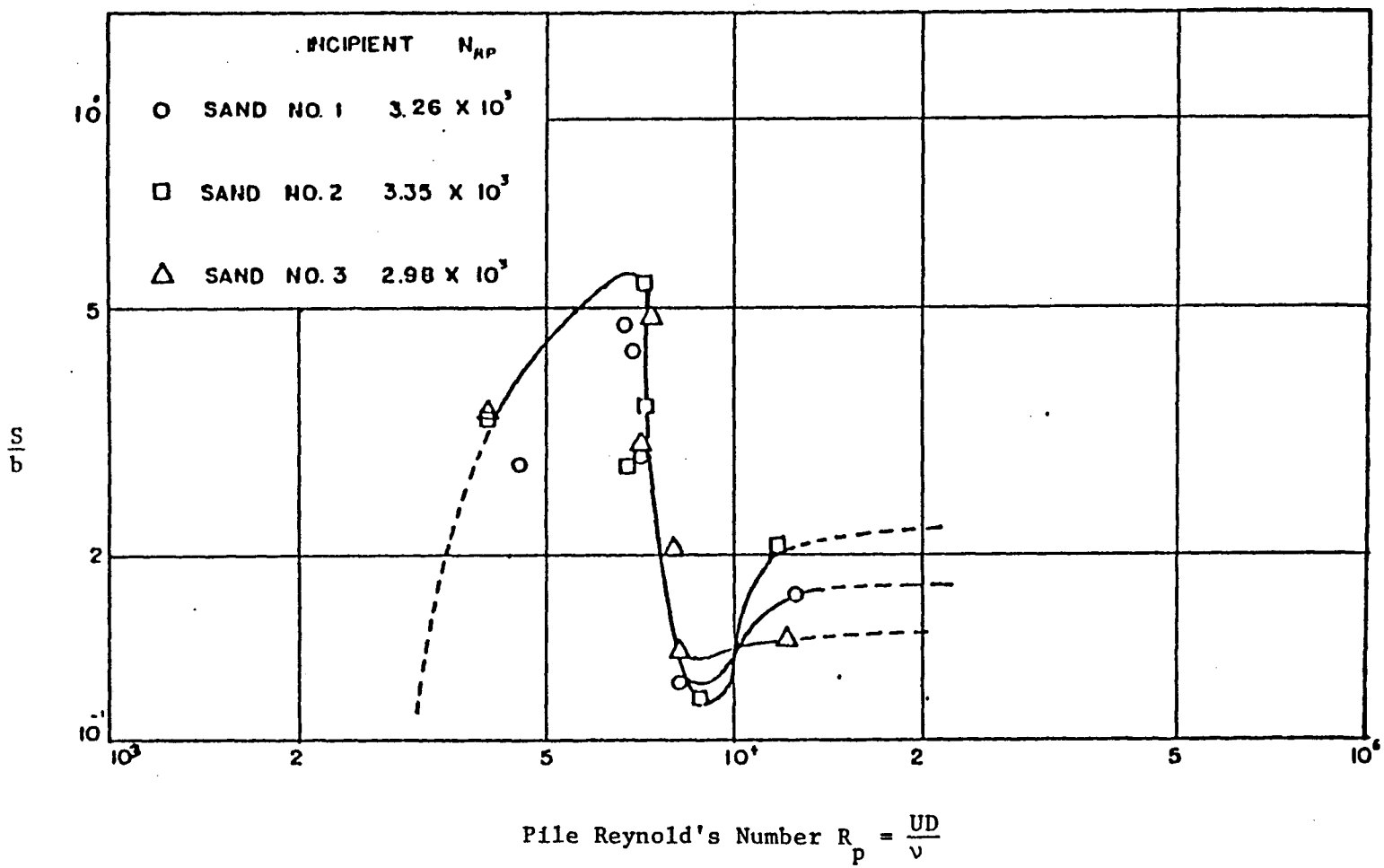

Figure 1.8. Relative scour versus Pier Reynold's number, Wells and Sorensen (1970).

continues to grow. The stability of a structure placed in a non-cohesive seabed may be heavily dependent upon the magnitude of scour experienced at the structure foundation. There have been many field observations describing the amount of scour that can occur at a structure's base. A few of these observations have been noted by Johnes (1970). He reported scour depths of 11 feet around the foundation piling of Diamond Shoal Lighthouse off the Coast of North Carolina. Also in North Carolina, the State Port Authority at Morehead City experienced the collapse of a waterfront warehouse. Direct exposure to waves and tidal currents was the cause of the failure in June 1962. For steady flow the flood of the Beaver River in Alberta, Canada caused excessive scour around the La Corey Bridge and the Beaver Crossing Bridge. Neill (1964b) reported a scour depth of 10 feet at the La Corey Bridge and 17 feet at the Beaver Crossing Bridge.

Abad and Machemehi (1974) studied scour due to combined waves and currents. They concluded that scour increases with an increase of wave length, but their tests were limited in scope and this increase would not be expected to continue when general sediment motion occurred.

Armbrust (1982) in his experimental study described local scour produced by wave and current motion and the dependency of scour around structures on flow characteristics.

Wang and Herbich (1983) introdued a complex parameter and for their range of tests the scour depth is related to this parameter by a certain formula. The parameter is formed by multiplying together five dimensional groups which are derived from their dimensional analysis, but no justification was made for making such an assumption. This parameter is a function of stream velocity to the power four and wave height to the

same power. It can be seen that scour depth according to their assumption is not limited, i.e. the scour depth will increase with current velocity and wave height increase which is not true once the threshold conditions have been exceeded. This formula is limited to the test conditions and reliable in that range only. The findings of the present study indicate that their formula should be used with great care. In conclusion, the majority of scour studies conducted in the past dealt with scour due to steady currents. In the last two decades some work has been done on the scour resulting from oscillatory wave motion. To date, only limited work, as cited above, has been conducted involving both waves and currents.

1.2.5 SCOUR DEPTH PREDICTION FORMULAS

In the case of pure waves and waves plus currents, no theoretical formula exists for estimating the scour, but some empirical relations exist which relate depth of scour to various flow parameters. For unidirectional flow - steady currents -, numerous references on local scour experiments on piers can be found in literature. Few of them, however, cover a sufficiently general range of conditions with independent variation of parameters. In most cases velocities were below or at the critical velocity for initiation of motion. Some of the interesting references are summarized below.

1) Larras (1963, 1960) analyzed the data given by Chabert and Engeldinger (1956). He concentrated on the maximum scour depth near the threshold velocity of the undisturbed material and gave a relation expressing scour depth as a function of pier diameter, with water depth and grain size neglected:

$$d_{sm} = 1.05\ b^{0.75} \tag{1.1}$$

where

d_{sm} = maximum possible scour depth

b = pier diameter

2) Hincu (1965) gave experimental results for circular piers (b = 3, 4.7, 6, 13, and 20 cm) in coarse material (D_{50} = 0.5, 2 and 5 mm). The scour depth was constant ($d_s = d_{sm}$) above a certain critical velocity (u_{cr}). At lower velocities a linear relation with velocity obtained

$$\frac{d_s}{d_{sm}} = \left(\frac{2U}{U_{cr}} - 1\right) \tag{1.2}$$

The influence of water depth was negligible for d/b > 1. The results were correlated with the expression:

$$\frac{d_{sm}}{b} = 2.42\ \left(\frac{U_{cr}}{gb}\right) \tag{1.3}$$

with a relation given for u_{cr}:

$$U_{cr} = 1.2\ \sqrt{gD\left(\frac{\rho_s - \rho}{\rho}\right)\left(\frac{d_o}{D}\right)^{0.2}} \simeq 1.54\ D^{0.3}\ d_o^{0.2}\ g^{0.5} \tag{1.4}$$

for natural sands, the relation may be converted into:

$$\frac{d_{sm}}{b} = 3.3\ \left(\frac{D}{b}\right)^{0.2}\ \left(\frac{d_o}{b}\right)^{0.13} \tag{1.5}$$

where

d_o = water depth

U = steady flow velocity

D = sediment size

3) Shen, Schneider, Karaki (1966a, 1969), Roper, Schneider, Shen (1967), Shen (1971) concluded that the maximum local scour near critical velocity for initiation of sediment will be:

$$d_{sm} = 0.00022\ Re^{0.619} \qquad \text{(m - units)} \qquad (1.6)$$

$$d_{sm} = 2\ Fr^{0.43}\ (\frac{d_o}{b})^{0.355} \qquad (1.7)$$

where

Re = Reynold's number

Fr = Froude number

4) Laursen and Toch (1956) suggested that d_{sm} changes with time for $U > U_{cr}$ and his formula may be presented as:

$$\frac{d_{sm}}{b} = 1.35\ (\frac{d_o}{b})^{0.3} \quad \text{for circular piers} \qquad (1.8)$$

Most of the above equations give maximum possible scour as a clear water scour near or at the threshold of motion in the approaching flow. Scour depth does not increase with steady flow velocity U for $U > U_{cr}$, as given by Chabert and Engeldinger (1965) but, in fact, decreases slightly, as reported by Chabert and Shen (1956, 1965).

2. THRESHOLD OF MOTION

The term threshold defines a limiting condition which forms the boundary between one state of affairs and another. Like many threshold conditions the threshold of sediment motion cannot be defined with absolute precision. Eagleson and Dean (1961) described the threshold of movement as, "a state of flow reached when the resultant of all active forces of the particle intersect the line connecting the bed particle contact points". Some of these active forces will be discussed later.

In this study threshold was assumed to correspond to a moderate number of particles moving. If threshold is assumed to correspond to very few particles moving, this motion is usually just a few small or light particles, which are soon removed, and the motion then ceases. Therefore a slightly more active particle movement is a more true threshold which will be maintained, and will not cease.

It is generally accepted that a fluid flowing over a sediment bed exerts a shear stress on the particles which causes them to move if it is sufficiently large. This shear stress at which the particles begin to move is known as critical shear stress, and is associated with a fluid velocity known as the critical velocity.

Usually, the Shields entrainment function (Shields, 1936) is used to define the shear stress for initial particle movement, but experimental results plotted on the Sheilds diagram show considerable scatter. This scatter may be attributable to such factors as the random shear stress exerted by the moving fluid, the random shear stress necessary to move bed particles, and each observer's definition of critical movement (Williams and Kemp, 1971). Despite the scatter, the Shields curve

remains about the best indicator of critical motion; details of the Shields criterion will be given later.

Bagnold (1946) has done a famous experiment using a sand bed on an ocillating plate to find critical motion. Komar and Miller (1974) have placed his oscillatory data on the unidirectional flow Shields diagram and have concluded that the Shields curve works well for oscillatory flow. This finding has been confirmed by Madsen and Grant (1975) and is an important advancement in the study of the onset of motion under waves.

Observations of sediment movement threshold seems to indicate that the shear stress is not the only factor in the mechanism, but there is another mechanism involved in the initiation of particle movement. The mechanism is the flow turbulence near the particles, though a quantitative description of the importance of flow turbulence is unavailable. It is apparent that the turbulence plays a role in the onset of threshold. Three primary active forces involved and relationship to incipient motion shall be discussed.

2.1 HYDRODYNAMIC FORCES

The forces influencing bed particle motion are hydrodynamic and consist of the forces of steady flow drag, lift and the so-called inertia forces of accelerating flow as proposed by Morison et al. (1950). However since the force due to inertia is a function of body volume (particle diameter D^3 in this case) which is very small hence it will never predominate and therefore it will be neglected. The total hydrodynamic force will be the combination of the lift force and the drag force. The hydrodynamic forces are opposed by the force of gravity and by frictional forces.

2.1.1 DRAG

Due to viscosity and boundary layer effects a separation of flow occurs on the boundary of the object and a wake is formed. The point of separation is a function of the shape of the object and the local Reynold's number. The drag force is the combination of form drag due to pressure differential and the viscous drag due to skin friction. For different bodies, one type of drag may dominate the other, as in the case of a perfect sphere when the total drag is primarily pressure drag. The point through which the drag force acts depends on the relative magnitude of the lift and drag force components which are functions of bed particles geometry, location, and local Reynold's number. The steady force due to drag as developed in any elementary fluid mechanics text can be shown to be equal

$$F_D = \frac{C_D}{2} \rho A U_c^2 \qquad (2.1)$$

where A is the projected area of object normal to flow direction, C_D is the drag coefficient, ρ is the fluid density and U_c is the free stream velocity. Since drag is a viscous phenomena, the coefficient of drag is primarily influenced by the Reynold's number. The drag coefficient for spheres has been studied by various authors. Drag is measured using fall velocity data. Under steady state conditions the fall velocity is called the terminal velocity and the drag on the particle is equal to the submerged weight. Therefore for a sphere,

$$C_D = \frac{(4/3)\, g\, D}{V} \left(\frac{\rho_s - \rho}{\rho}\right) \qquad (2.2)$$

where V is the fall velocity, D is the particle size diameter, g is the gravity and ρ_s is the density of sediment.

Alger and Simons (1968) adjusted the sphere drag coefficient for irregular shaped particles through the use of shape factor,

$$SF \frac{d_A}{d_n} \tag{2.3}$$

where SF is Corey shape factor = $c \sqrt{ab_o}$, a is the maximum dimension of the particle, b_o is the intermediate dimension of the paticle, c is the minimum dimension of the particle, d_A is the diameter of a sphere having the same surface area as the particle and d_n is the diameter of a sphere having the same volume as the particle. The drag coefficient increases as the shape factor increases for the same Reynold's number. It is not only a function of Reynold's number, but also particle geometry, and is also influenced by adjacent particles as pointed out by White (1940).

2.1.2 LIFT

The relationship for the force due to lift is similar to that for form drag and is given by

$$F_L = \frac{C_L}{2} \rho A U_c \tag{2.4}$$

where F_L is the lift force and C_L is the lift coefficient. Since the fluid is passing above a particle, there is a decrease in pressure above the particle, whereas below the particle the pressure remains fairly hydrostatic. Although the lift is very difficult to measure, but it can be taken in consideration among the drag force since both of them are functions of U_c^2.

2.1.3 GRAVITY

The hydrodynamic forces are opposed by the weight of the particles and friction. The friction is usually expressed in terms of friction angle - angle of natural repose -, and the gravity force may be simply expressed as the particle's submerged weight. The submerged weight of a perfect sphere is given as

$$F_g = \frac{\pi}{6} D^3 (\gamma_s - \gamma) \tag{2.5}$$

where F_g is gravitational force, D is the sphere diameter, γ_s is the unit weight of the sphere and γ is the unit weight of the fluid.

Figure 2.1 shows the three primary forces on a hypothetical sand particle. When these hydrodynamic forces acting on a grain of sediment reached a value that, if increased even slightly the grain will move, critical or threshold conditions are said to have been reached. Under these critical conditions the hydrodynamic forces are just balanced by the resisting force of the particle, i.e., the sum of the moments about the contact point of F_g and F_T equals zero.

White (1940) studied the equilibrium of a particle in laminar flow and defined a critical shear stress as:

$$\tau_{cr} = 0.18 (\gamma_s - \gamma) D_s \tan\phi \tag{2.6}$$

for turbulent flow, the drag force is

$$F_D = \tau_o C_2 D_s^2 \tag{2.7}$$

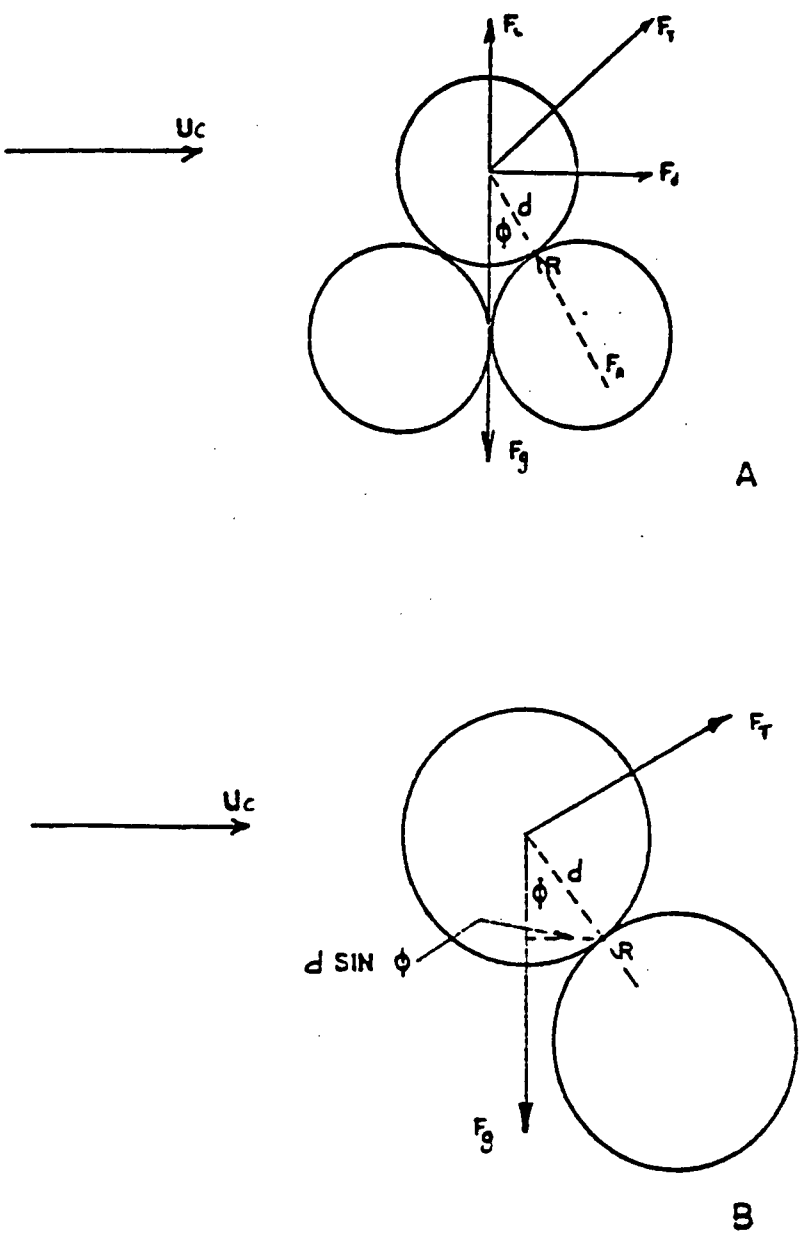

Figure 2.1. Primary forces acting on an individual sand particle, Wells and Sornesen (1970).

where τ_o is the bed shear stress, D_s is a characteristic diameter of the particle, $C_2 D_s^2$ is the effective surface area of the particle exposed to the shear stress τ_o, τ_{cr} denotes the critical shear stress and C_2 is a form coefficient defining the effective surface area of the particle, that is the area of the projection of the particle on a plane perpendicular to the direction of the fluid flow. For the critical conditions $\tau_o = \tau_{cr}$.

For fully turbulent flow considering the drag and the lift force

$$\tau_{cr} = \frac{(\gamma_s - \gamma)}{\frac{C_L}{C_1} + \frac{C_2}{C_1} \cot \phi} \tag{2.8}$$

or

$$\frac{\tau_{cr}}{(\gamma_s - \gamma) D_s} = \frac{1}{k_1 + k_2 \cot \phi} \tag{2.9}$$

where $k_1 = \frac{C_L C_4}{C_1}$, $k_2 = \frac{C_2}{C_1}$

$$C_4 = \frac{C_3}{2} \left(\frac{C_1}{C_2}\right)^2 .$$

C_1 is a form coefficient, C_2 and C_3 are form coefficients related to the effective surface area of the particle in the direction of the drag and the lift force respectively and ϕ is the angle of repose of the submerged sediment. If $C_L = 0$, equation (2.9) reduces to

$$\frac{\tau_{cr}}{(\gamma_s - \gamma) D_s} = \frac{C_1}{C_2} \tan \phi \tag{2.10}$$

The parameter $\frac{\tau_{cr}}{(\gamma_s-\gamma)D_s}$ is the ratio of the drag force to the gravitational force, often referred as Sheilds parameter. Hence, this dimensionless number is a type of Froude number that is related to the grain size and the shear velocity. A dimensional analysis yields

$$\frac{\tau_{cr}}{(\gamma_s-\gamma)D_s} = \frac{\rho\, U^*_{cr}}{(\gamma_s-\gamma)D_s} \tag{2.11}$$

hence

$$\tau_{cr} = \rho\, U^{*2}_{cr} \tag{2.12}$$

where U^*_{cr} is the shear velocity at the threshold condition.

2.2 ANALYSIS OF THE SHIELDS CRITERION

The Shields curve (Figure 2.2) has been based on experiments in laboratory flumes with fully developed two-dimensional flows over flat sediment bed. For the turbulent boundary layer, a logarithmic velocity profile had been assumed, and in defining the critical shear stress values on the bed for initial particle movement, Sheilds used the temporal mean shear stress. The critical shear stress was obtained by extrapolating a graph of observed sediment discharge versus shear stress and it does not depend on a qualitative criterion (Task Committee, 1966).

The Task Committee Report revealed that one of the main reasons for the data scatter on the Shields diagram stems from the difficulty

encountered in consistently defining critical flow conditions. Consistency is difficult to achieve because of the random shear stress exerted by the moving fluid, and because of the random particle susceptibility to movement under a local instantaneous shear stress.

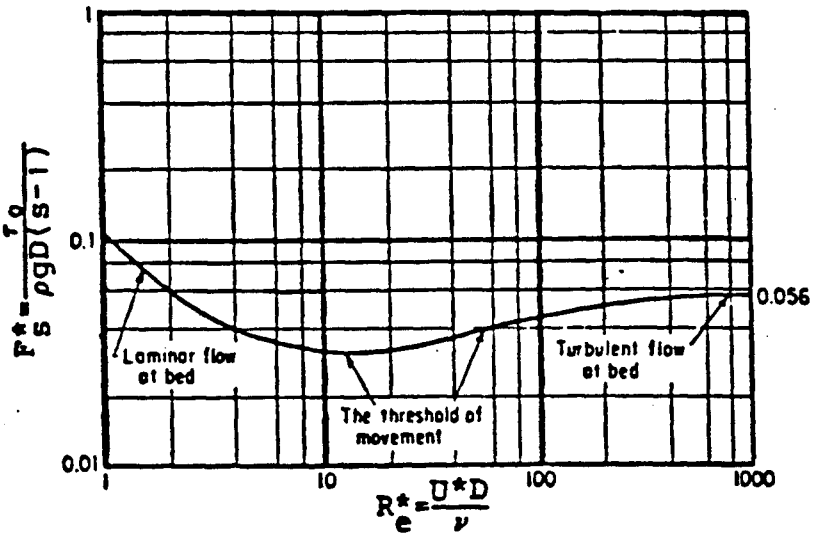

Figure 2.2. The Shield's entrainment function.

The exerted shear stress is random because of the turbulence in the fluid flow, and any instantanteous shear stress is a function of the temporal mean shear stress, the fluid density and viscosity and the flow boundary conditions including the particle geometry.

The particle susceptibility depends on the shape, weight, and placement of any particle, and the overall particle susceptibility can be described by a probability distribution (Grass, 1970).

There is the problem of different observers having different perceptions as to the onset of sediment motion. Some may predict motion when the very first grains are in movement, and others not until a substantial fraction of the bed particles are in motion.

A further problem is caused by the use of different wave flumes. Grass explained that because different wave flumes have different boundary conditions, the boundary region turbulence are necessarily different and they no longer show similarity with respect to the average critical shear stress values derived from the Shields curve.

2.3 THRESHOLD MEASUREMENTS

Much work has been done on the threshold under unidirectional steady current conditions. The finding of Shields (1936) is universally accepted as the fore-runner in sediment entrainment studies. Bagnold (1966) has presented a curve similar to that of Shields, but presented in a more convenient form having replaced the particle Reynold's number with the particle diameter (Figure 2.3).

Much work has been done in determining the sediment movement threshold under oscillatory flow conditions. Komar and Miller (1974) found from the data of previous researchers that the sediment entrainment conditions are simliar for all types of oscillation investigated. These conditions have been attained by use of waves in flumes, oscillatory water tunnels, and oscillatory plates. Prototype periods, orbital diameters, and orbital velocities cannot be reproduced in wave tests in ordinary tanks because the period is so restricted. The other methods are able to generate these prototype conditions, but may not be able to recreate the prototype pressures and convective accelerations as experienced under waves.

Komar and Miller (1974) reported that these methods of generating an oscillating flow over a sediment bed lead to the similar conclusion that the shear stress required to move sediment under waves is the same as

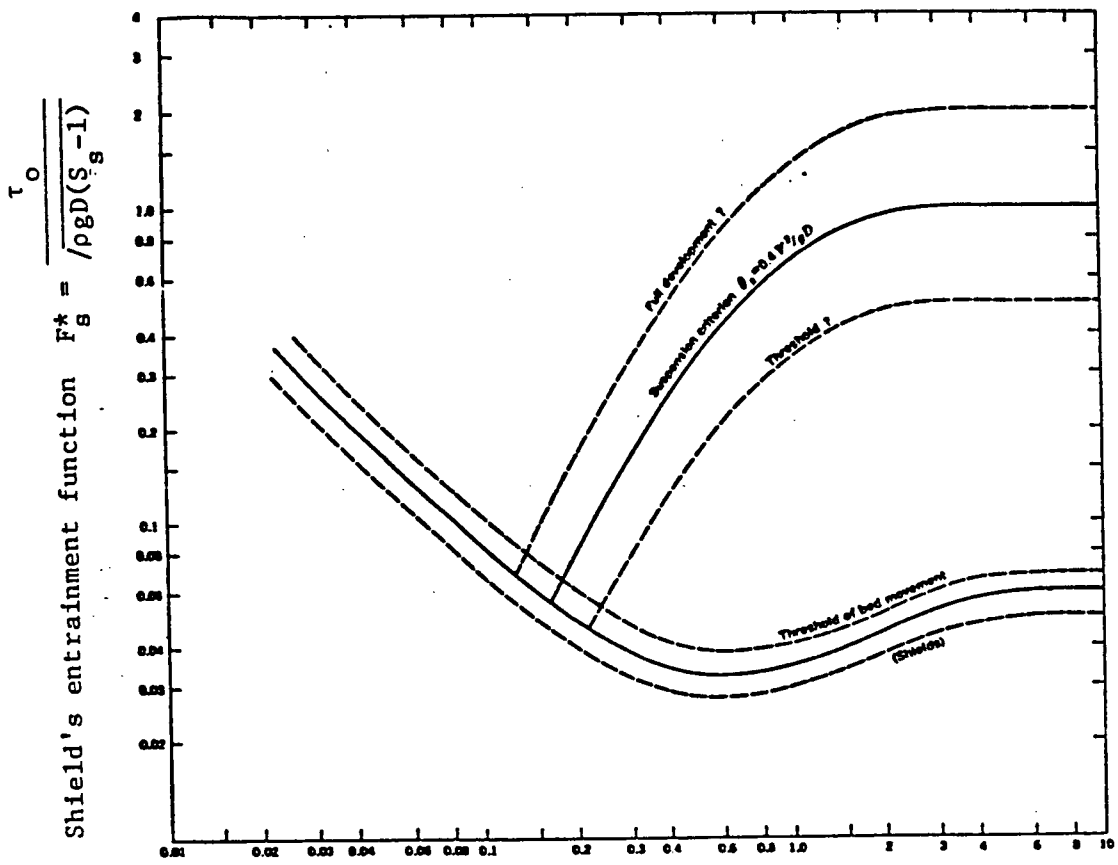

Figure 2.3. Modified Shield's diagram after Bagnold (1966).

that required to move sediment under a unidirectional current. Komar and Miller used five sets of published data in analysis of the threshold. Bagnold (1946) and Monohar (1955) used oscillatory plates, Rance and Warren (1969) used an oscillating water tunnel, while Horikawa and Watanabe (1967) nad Eagleson, Dean and Peralata (1958) used waves in a wave flume. The last two sets of data were not used much except to support the conclusions as determined using the first three data sets.

The sediment particle diameters range from 0.009 to 4.8 cm, and their densities from 1.52 to 7.9 gm/cm^3. The data points obtained range over the entire spectrum of Reynold's number used in the Shields diagram, so a complete comparison of the unidirectional and oscillatory critical shear stresses is possible.

Madsen and Grant (1975, 1976) demonstrated that Shields criterion for the initiation of sediment movement as derived from steady unidirectional flow conditions serves as quite an accurate and general criterion for the initiation of sediment movement in oscillatory flow provided that the boundary shear stress is properly evaluated.

Quick et al. (1985) have studied the onset of sediment motion under combined waves and steady currents. They assumed that the threshold of sediment motion represents a critical level of shear stress at the bed and they concluded that a similar maximum velocity condition, measured very close to the bed, causes onset of motion for all the conditions tested, currents, waves, and combined waves plus currents. The study assumed that the near bed maximum wave and average current velocity at one roughness height above the bed combine linearly and show to be in reasonable agreement with Shields threshold criterion for steady current; the result of that study for the maximum velocity criterion is shown in Table 2.1 and Figure 2.4.

Sediment Size m.m.	Measured Maximum Velocities cm/sec			Shear Velocities cm/sec			Calculated Maximum Velocities (Eqt.9)		
	Current	Wave	Wave & Current	From Manning	Shields(1) for Man. D	Shields(2) for Min. D	Manning	Shields(1)	Shields(2)
0.3 - 0.85	26.7	26.7	27.6	1.71	2.12	1.38	29.7	24.6	25.9
0.85 - 1.16	29.7	28.7	29.5	2.11	2.31	2.12	24.3	28.9	24.6
1.16 - 1.70	32.4	31.3	32.8	2.46	3.24	2.51	30.6	37.3	28.9
1.70 - 2.00	35.4	34.9	35.9	3.05	3.61	3.24	35.1	41.5	37.3
2.00 - 2.35	36.9 (33.6)	39.2	38.2	3.21	4.04	3.61	36.9	46.5	41.5

Table 2.1. Shear velocities and maximum near-bed velocities after Quick et al. (1985).

It should be emphasized that some of the previously mentioned results obtained are usually limited by the range of experimental conditions from which they were derived and are not of the general nature of the Shields criterion for unidirectional steady flow.

It is therefore concluded that the Shields Criterion for onset of sediment motion is a good tool to determine the level of critical shear stresses at which particles start to move, bearing in mind a representative size of the sediment size range.

As shown by Quick et al. (1985), the Shields Criterion can be extended for any kind of flow, since the critical shear stresses at threshold conditions will be almost the same whether it was attained by steady currents alone or waves alone or combined waves and currents.

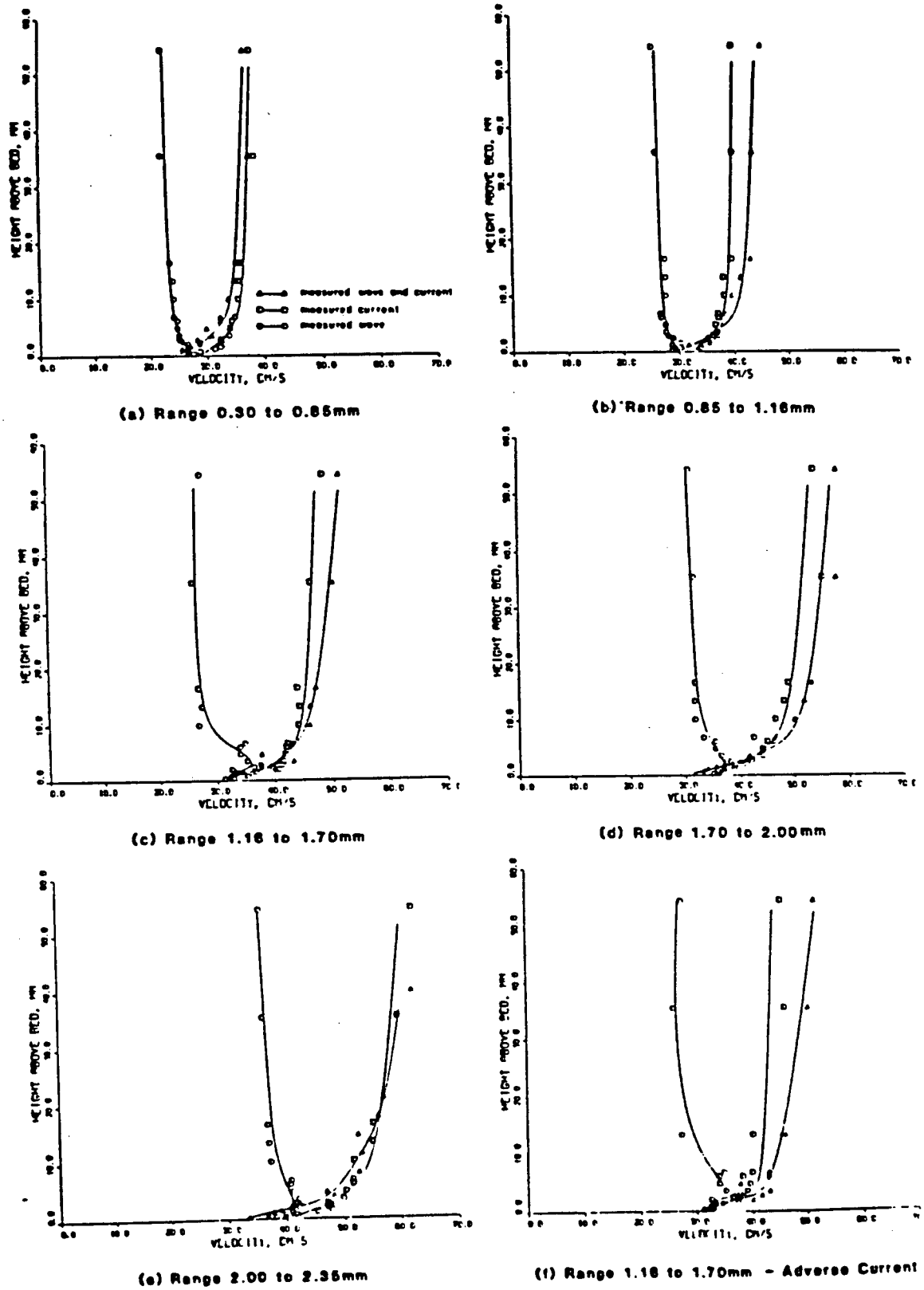

Figure 2.4 Measured threshold velocity profiles after Quick et al. (1985).

3. THEORETICAL BACKGROUND

3.1 WAVE AND CURRENT INTERACTION

A basic understanding of wave current interation is fundamental for studying scour under combined waves and currents. Waves and currents interact in two ways. The first is the modification of a wave which travels from a zero region to a region where currents exist. The second is the behaviour of a wave which is already superimposed on a current; for this situation the resultant is a simple combination of the wave and the current flow fields.

As discussed by Quick (1983), the major features of the wave and current combination problem can be defined by transforming the situation of a wave on a uniform current into an exactly similar wave on water at rest. This transformation is achieved simply by subtracting the uniform current as shown in Figure 3.1. The wave height and length are unaltered, but the wave period is now T_r, on zero current. The velocity field of the equivalent wave can then be analyzed using standard wave

Figure 3.1. Definition sketch for a progressive wave train on a steady current.

theory. This argument is confirmed by Kemp and Simons (1982); they concluded that comparison with theoretical profiles suggests that the addition of a current on a wave has little effect on the close agreement between the measured waves and those of both second- and third-order theory, provided that the wave period is reasonably adjusted.

Figure 3.2 allows further comparison, by plotting equivalent profiles of the same waves with and without currents. Referring to Figure 3.1, the following equations hold:

$$L = C_a T_a = C_r T_r \tag{3.1}$$

$$C_a = C_r + U_c \tag{3.2}$$

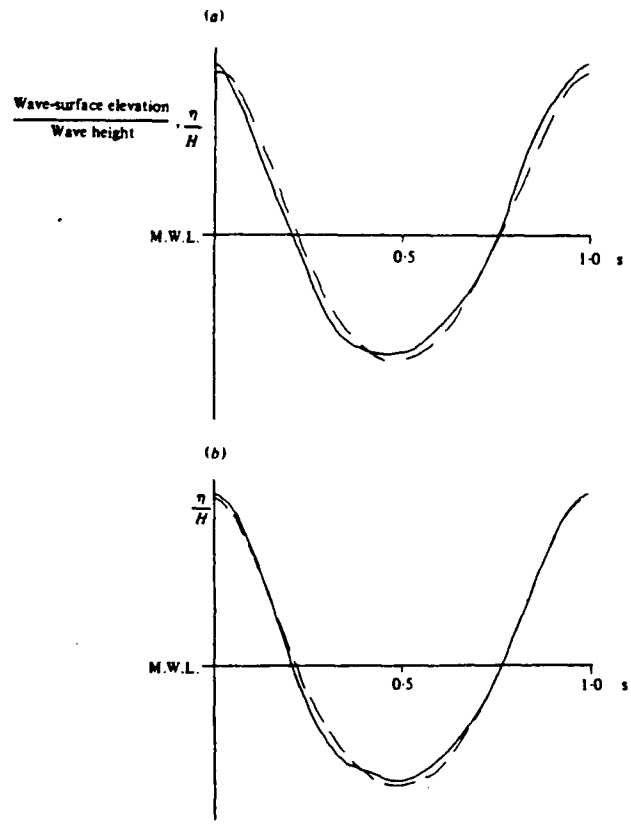

Figure 3.2. Wave profiles with and without current. (a) Rough boundary layer; (b) smooth boundary layer. ——, wave with current; ---, wave alone, Kemp and Simons (1982)

$$T_r = \frac{L\,T_a}{L - U_c T_a} \tag{3.3}$$

where L is the wave length, T is the wave period, C is the wave celerity, and U_c is the steady current velocity. The subscripts 'a' and 'r' refer to the absolute and relative coordinate with the current, respectively.

Many investigators have attempted to give a full explanation of how the presence of a wave can affect the steady current boundary layer which is important when modelling problems. Most of these studies rely on mathematical or theoretical models for the wave current interaction and attempt to find theoretical relations for near bottom velocities and consequently for shear stress estimation.

Grant and Madsen (1979) presented an analytical theory to describe the combined motion of waves and currents in the vicinity of a rough bottom and the associated boundary shear stress. Characteristic shear velocities were defined for wave and current boundary layer regions by using a combined wave-current friction factor 'f_{cw}' which was given in a very complex form. The maximum bottom shear stress $|\tau_{b,max}|$ is given as,

$$|\tau_{b,max}| = \frac{1}{2} \quad f_{cw}\, \rho\, \alpha\, |U_b|^2 \tag{3.4}$$

where

$$\alpha = 1 + (|U_a|/|U_b|)^2 + 2(|U_a|/|U_b|)\cos\phi_c \tag{3.5}$$

where $|U_a|$ is the magnitude of the steady current velocity vector at a height a above the bottom; $|U_b|$ is the maximum near-bottom orbital velocity from linear wave theory, and ϕ_c is the angle made by U_a with the direction of wave propagation.

Brevik and Aas (1980) studied three aspects of wave-current behaviour. Firstly they studied the wave amplitude variation when a periodic wave, initially on still water, propagates into a following or an opposing current, fed from below. Secondly they investigated wave attenuation on homogeneous currents or on still water and the results were used to determine the appropriate bed friction factor. Thirdly, the horizontal fluid velocity components in a wave-current system were measured. They gave the wave-current friction factor f_{wc} as a function of wave attenuation factor $\frac{d}{dx}(H)$ along the wave flume; in the limiting case for pure waves, this friction factor is close to Jonsson's factor.

Kemp and Simons (1982,1983) concluded that unidirectional turbulent boundary layer is reduced in thickness by the superposition of waves propagating with current on both rough and smooth bed sand within 2 roughness heights of the roughbed. The turbulence characteristics are dominated by the periodic formation of vortices at the bed. According to them the shear stress measurements under waves alone are in a good agreement with values estimated using wave friction factors fw (Jonsson) calculated from $\frac{1}{4} f_w^{-1/2} + \log_{10} (\frac{1}{4} f_w^{-1/2}) = \log_{10} (a_{om} k_s^{-1})$ and f_w (Kajiura) calculated from $fw = 0.37 (a_{om}/k_s)^{-2/3}$ where a_{om} is the maximum wave displaement at bottom estimated using potential wave theory and k_s is the roughness size. Fredsoe (1984) calculated the mean current velocity in the combined wave-current motion.

3.2 NEAR-BOTTOM SHEAR STRESSES

3.2.1 UNIDIRECTIONAL FLOW SHEAR STRESSES

The shear stress at bed under unidirectional flow is given by the well known formula

$$\tau_o = \rho U_c^{*2} \tag{3.6}$$

where τ_o is the shear stress at bed, ρ is the fluid density and U_c^* is the shear velocity of the free stream. This formula has been in use for long time and it has been checked against laboratory and field measurements. The mean current velocity near the bed can be calculated using the Manning-Strickler relationship which is based on a wealth of rough boundary steady flow open channel measurements. This equation can be re-written in terms of shear velocity U_c^* and the sediment or roughness size D, by using the relationships (Henderson, 1966)

$$n = 0.038\ D^{1/3} \qquad \text{(d in meters)} \tag{3.7}$$

$$U_c^{*2} = g\ R_h\ S_o \tag{3.8}$$

Then the Manning equation becomes,

$$U_c = 8.4\ \left(\frac{R_h}{D}\right)^{1/6} U_c^* \tag{3.9}$$

where U_c is the mean current velocity, R_h is the hydraulic radius, D is the sediment size, n is the Manning's roughness coefficient and S_o is the bed slope. For a given mean velocity, flow cross section and sediment size, the equation yields quite robust estimates of U_c^*.

3.2.2 OSCILLATORY FLOW SHEAR STRESSES

The near-bottom shear stress due to oscillatory flow is expressed as:

$$\tau_w = \frac{1}{2} f_w \rho U_{1m}^2 \qquad (3.10)$$

τ_w is the shear stress at bottomn due to pure wave motion, f_w is a friction factor for τ_w, and U_{1m} is wave particle velocity at the bottom. The friction factor f_w is a function of the type of flow, laminar or smooth or rough turbulent regimes, and also function of the bed roughness. There are many formulas in the literature for predicting the friction factor, see for instance Kajiura (1968), Jonsson (1966) and Kamphius (1975). Under natural conditions, the bed boundary layer below sea waves is often rough turbulent, see Brevik (1981) and Fredsoe (1984).

3.2.3 COMBINED SHEAR STRESSES AT BED

The shear stresses under combined waves and currents can be estimated in different ways, assuming a simple combination of the flow fields, that is a linear addition of the velocity fields, including both the mean and turbulent components. If the flow is turbulent, such a linear addition of flow fields would result in a nonlinear combination of shear stresses

$$\tau_{wc} = \tau_w + \tau_c + \sqrt{2\ \tau_w \tau_c} \qquad (3.11)$$

where τ_{wc} is the near bed shear stress due to combined waves and currents, τ_c is the steady current shear stress, and τ_w is the oscillatory flow shear stress. This agrees with Quick et al. (1985) results. The near-bottom shear stress can be estimated using what will be called equivalent or characteristic shear velocity U^*_{wc}. The shear stress in this case will be defined as:

$$\tau_{wc} = \rho \, (U^*_{wc})^2 \tag{3.12}$$

Tanaka and Shuta (1984) in their paper found out that shear stress for combined wave and current is given as:

$$\tau_{wc} = \frac{1}{2} \rho \, f_{wc} \, U^2_{1m} \tag{3.13}$$

where f_{wc} is a friction factor under combined wave and current and U_{1m} is the amplitude of horizontal velocity of the oscillating component just outside the boundary layer. It may at first appear somewhat curious that Equation (3.13) explicitly contains only the unsteady velocity component. However because f_{wc} calculation includes the steady current component, the definition in Equation (3.13) is not unreasonable. The f_{wc} can be calculated using the flow chart diagram as shown in Figure 3.3. The terms in the flow chart are:

U_w is the maximum value of horizontal velocity of the unsteady component, a_m is the horizontal excursion length of a water particle in oscillatory moton given by potential theory, z_h is the depth of flow, z_o is the roughness length, σ is the angular velocity, ν is the kinematic viscosity, τ_{om} is the maximum bottom shear stress, ρ is the fluid density, R_a is the Reynold's number and equal $U_w a_m/\nu$, R_c is the Reynold's number and equal $\bar{U}_c z_h/\nu$, $\bar{U}_c$ is the horizontal velocity of the steady component, and f_{wc} is the friction coefficient for a wave-current coexisting system, noting that U_w is given by the following formula

$$U_w = \frac{(\frac{\pi H}{L})(\frac{L}{T} + \bar{U}_c)}{\sinh (2\pi \, z_h/L)} \tag{3.14}$$

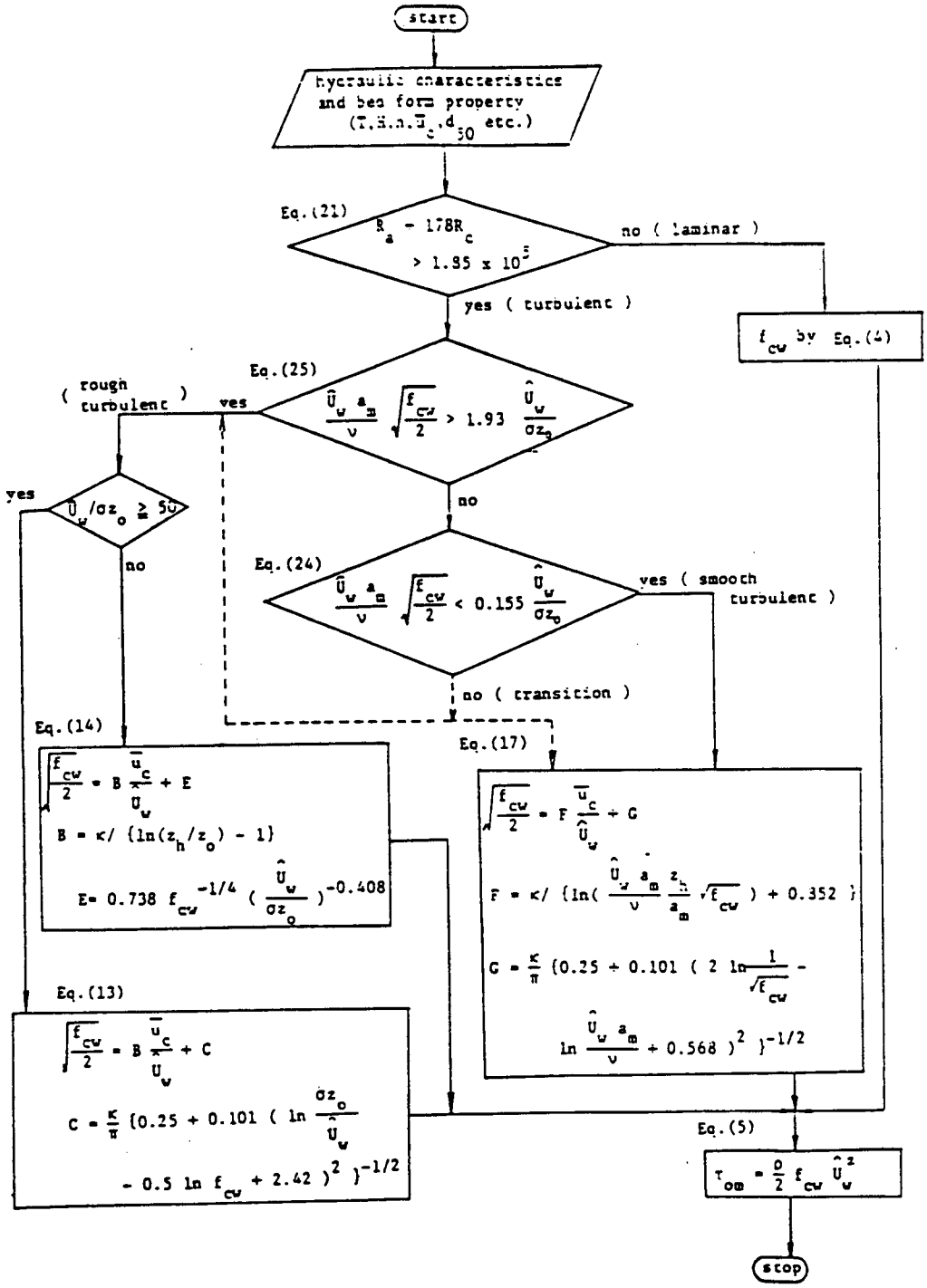

Figure 3.3 Flow chart diagram for calculation of f_{wc} after Tanaka and Shuto (1984).

where H is the wave height, L is the wave length, and T is wave period. The compound sign is positive for opposing flow and negative for following flow. For $\bar{U}_c/U_w = 0.0$, i.e., for pure waves, the friction coefficient obtained by this method is almost identical with that of Jonsson (1966).

3.2.4 SHEAR STRESSES COMPARISON

The shear stress calculations due to different methods are given for three sediment size ranges for waves plus currents at threshold condition, see Table 3.1, noting that the roughness height is the upper limit of the sediment size range.

Method No. \ Sediment Size Range (mm)	0.3 - 0.85	0.85 - 1.16	1.16 - 1.7
1	0.576	0.658	0.814
2	0.702	0.838	1.061
3	0.450	0.630	1.050
4	0.550	0.720	1.370
5	0.380	0.520	1.000
6	0.620	0.820	1.570

Table 3.1 Combined wave and current shear stresses in (Pa) due to different methods for three sediment sizes at threshold conditions.

The different methods are summarized below:

Method 1: using the equivalent shear velocity concept as given by Equation (3.12)

Method 2: using the friction factor f_{wc} given in Figure 3.3.

Method 3: using Shields criterion for threshold conditions.

Method 4: shear stresses using Jonsson's shear factor f_w given as

$$\frac{1}{4\sqrt{f_w}} + 10g_{10}\left(\frac{1}{4\sqrt{f_w}}\right) = -0.08 + \log_{10}\left(\frac{a_{1m}}{k_s}\right) \qquad (3.15)$$

for the unsteady component.

Method 5: using Kamphius' shear factor f_w given as

$$\frac{1}{4\sqrt{f_w}} + 10g_{10}\left(\frac{1}{4\sqrt{f_w}}\right) = -0.35 + \frac{4}{3}\log_{10}\left(\frac{a_{1m}}{k_s}\right) \qquad (3.16)$$

Method 6: using Kajiura shear factor f_w given as

$$\frac{1}{4\sqrt{f_w}} + \log_{10}\left(\frac{1}{4\sqrt{f_w}}\right) = -0.254 + 10g_{10}\left(\frac{a_{1m}}{k_s}\right) \qquad (3.17)$$

where

a_{1m} is the amplitude of horizontal particle motion just outside the boundary layer in oscillating flow, f_w is a friction factor for oscillatory flow, and k_s is the height of particle for equivalent sand roughness.

Referring to Table 3.1 it can be seen that most of the above mentioned methods give shear stress values close to each other especially for the small sediment size ranges. It is also seen that Method 1 using the equivalent shear velocity U^*_{wc} gives shear stresses estimation which is in good agreement with most of the other methods.

3.3 WAVE THEORIES

Wave theory requires an incompressible, inviscid fluid having irrotational flow. The wave train must be progressive and two-dimensional, travelling in water of constant depth as shown in Figure (3.4).

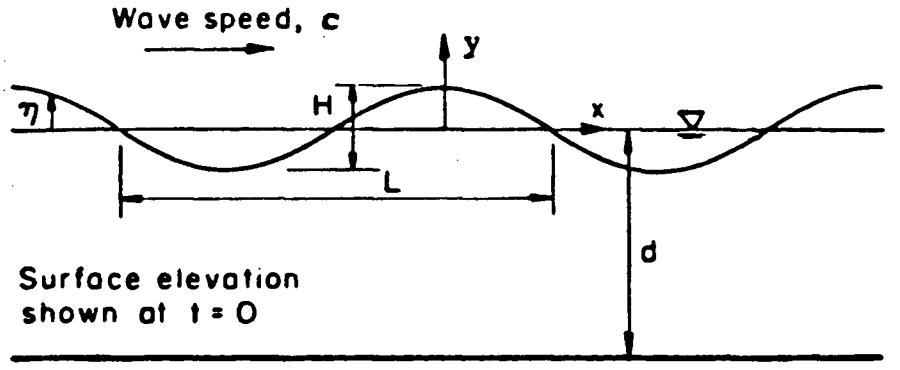

Figure 3.4 Definition sketch for a progressive wave train.

A choice of the most suitable wave theory is difficult to make. The first problem is that for a specific wave train, different wave theories will adequately reproduce different charateristics of interest. A comparison between theories must be made for a particular characteristic, and no generalization can be made regarding the comparison of these theories for other characteristics.

Another point to consider is that the most suitable wave theory may not be the one that is simply the most accurate. The governing criterion in a given engineering application may be to choose a theory that is simple and convenient to use, at the cost of some accuracy.

Based on the theoretical comparison of many investigators, Sarpkaya and Isaacson (1981) concluded that the stokes and cnoidal fifth order theories are sufficiently accurate for most engineering purposes, and yet are relatively simple to use. Fenton (1979) recommended that cnoidal

theory can be used for L/d > 8 and Stokes theory otherwise. For a detailed description of different wave theories, the reader is referred to Sarpkaya and Isaacson (1981), who described the well known and the less well known theories and some computation methods.

Quick et al. (1985) found out that, for the range of experimental tests, the near bottom velocities calculated by Stokes second order theory is in a reasonable agreement with the measured velocities, see Figure 3.5. The results of Stokes second order theory are presented in Table 3.2.

3.4 COEFFICIENT OF REFLECTION

In the wave flume, reflected waves from the energy absorbing end of the flume will have an influence on the water particle velocities. It is important to determine the amplitude of their contribution to the particle velocities near the bed.

The ratio of reflected wave height to incident wave height is designated by the reflection coefficient, K_r, where

$$K_r = H_R/H \tag{3.18}$$

where H_R is the height of the reflected wave, which travel in the opposite direction of the incident waves.

As shown by Sarpkaya and Isaacson (1981), the coefficient of reflection can be determined simply by traversing the flume in the direction of wave propagation with a wave probe to measure the maximum and the minimum wave height H_{max} and H_{min}, respectively. Then

$$K_r = \frac{H_{max} - H_{min}}{H_{max} + H_{min}} \tag{3.19}$$

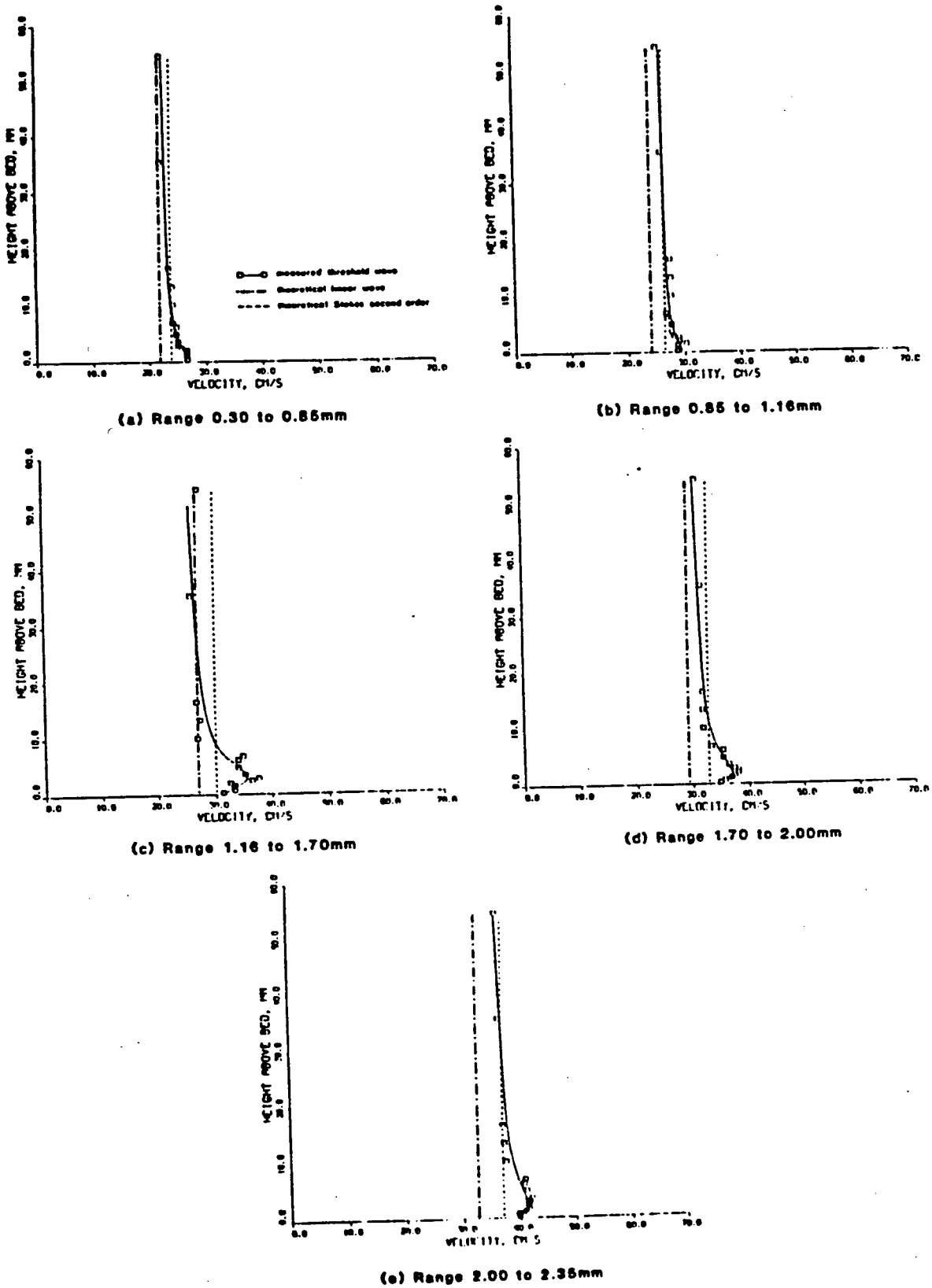

Figure 3.5 Measured and theoretical wave velocity profiles after Quick et al. (1985).

Velocity Potential	$\phi=\frac{\pi H}{kT}\frac{\cosh(ks)}{\sinh(kd)}\sin(\theta)$ $+\frac{3}{8}\frac{\pi H}{kT}(\frac{\pi H}{L})\frac{\cosh(2ks)}{\sinh^4(kd)}\sin(2\theta)$
Dispersion Relation	$c^2=\frac{\omega^2}{k^2}=\frac{g}{k}\tanh(kd)$
Surface Elevation	$\eta=\frac{H}{2}\cos(\theta)$ $+\frac{H}{8}(\frac{\pi H}{L})\frac{\cosh(ks)}{\sinh^3(kd)}[2+\cosh(2kd)]\cos(2\theta)$
Horizontal Particle Displacement	$\xi=-\frac{H}{2}\frac{\cosh(ks)}{\sinh(kd)}\sin(\theta)$ $+\frac{H}{8}(\frac{\pi H}{L})\frac{1}{\sinh^2(kd)}[1-\frac{3\cosh(2ks)}{2\sinh^2(kd)}]\sin(2\theta)$ $+\frac{H}{4}(\frac{\pi H}{L})\frac{\cosh(2ks)}{\sinh^2(kd)}(\omega t)$
Vertical Particle Displacement	$\zeta=\frac{H}{2}\frac{\sinh(ks)}{\sinh(kd)}\cos(\theta)$ $+\frac{3H}{16}(\frac{\pi H}{L})\frac{\sinh(2ks)}{\sinh^4(kd)}\cos(2\theta)$
Horizontal Particle Velocity	$u=\frac{\pi H}{T}\frac{\cosh(ks)}{\sinh(kd)}\cos(\theta)$ $+\frac{3}{4}\frac{\pi H}{T}(\frac{\pi H}{L})\frac{\cosh(2ks)}{\sinh^4(kd)}\cos(2\theta)$
Vertical Particle Velocity	$v=\frac{\pi H}{T}\frac{\sinh(ks)}{\sinh(kd)}\sin(\theta)$ $+\frac{3}{4}\frac{\pi H}{T}(\frac{\pi H}{L})\frac{\sinh(2ks)}{\sinh^4(kd)}\sin(2\theta)$
Horizontal Particle Acceleration	$\frac{\partial u}{\partial t}=\frac{2\pi^2 H}{T^2}\frac{\cosh(ks)}{\sinh(kd)}\sin(\theta)$ $+\frac{3\pi^2 H}{T^2}(\frac{\pi H}{L})\frac{\cosh(2ks)}{\sinh^4(kd)}\sin(2\theta)$
Vertical Particle Acceleration	$\frac{\partial v}{\partial t}=-\frac{2\pi^2 H}{T^2}\frac{\sinh(ks)}{\sinh(kd)}\cos(\theta)$ $-\frac{3\pi^2 H}{T^2}(\frac{\pi H}{L})\frac{\sinh(2ks)}{\sinh^4(kd)}\cos(2\theta)$
Pressure	$p=-\rho gy+\frac{1}{2}\rho gH\frac{\cosh(ks)}{\cosh(kd)}\cos(\theta)$ $+\frac{3}{4}\rho gH(\frac{\pi H}{L})\frac{1}{\sinh(2kd)}[\frac{\cosh(2ks)}{\sinh^2(kd)}-\frac{1}{3}]\cos(2\theta)$ $-\frac{1}{4}\rho gH(\frac{\pi H}{L})\frac{1}{\sinh(2kd)}[\cosh(2ks)-1]$
	$s=y+d$

Table 3.2 (Modified after Sarpkaya and Isaacson, 1981). Results of Stokes Second Order Theory.

and the incident wave height H is given by

$$H = 1/2\ (H_{max} + H_{min}) \tag{3.20}$$

In the wave flume used, the reflection coefficient was found to be less than 0.07.

3.5 SCALE EFFECTS

The improper scaling of the sediment size is usually accepted in a study of this type. Proper sediment size scaling would lead to a cohesive model sediment, and a cohesive sediment possesses properties vastly different from a non-cohesive sediment.

Wave damping due to the side walls will not pose a problem in this study since the wave properties will be measured at the test section.

According to Bijker (1967), the boundary layer resulting from a combination of current and waves is directly proportional to the boundary roughness, and thus the boundary friction factor. This implies that the boundary layer thickness for the model and the prototype will be approximately the same.

3.6 SOME IMPORTANT NUMBERS

3.6.1 FROUDE NUMBER

In the case of steady flows, Froude number F_r is defined by the following equation,

$$F_r = \frac{U_c}{\sqrt{gd}} \tag{3.21}$$

where d is the flow depth, and U_c is the steady current velocity. The Pier or Pile Froude number F_p is given as:

$$F_p = \frac{U_c}{\sqrt{gb}} \tag{3.22}$$

where b is the pier diameter.

3.6.2 REYNOLD'S NUMBER

Under unidirectional flow, Reynolds number Re is given as

$$Re = \frac{U_c\ r}{\nu} \tag{3.23}$$

where r is a characteristic length dimension; in case of open channels r is equal to the hydraulics radius R_h, and ν is the kinematic viscosity.

For piers or piles Reynold's number R_p is given in the form of:

$$R_p = \frac{U_c\ b}{\nu} \tag{3.24}$$

some references give it as

$$R_p = \frac{U_c\ b\ (\rho_s - \rho)}{\mu} \tag{3.25}$$

where $(\rho_s - \rho)$ is the sediment-fluid densty difference, and μ is the dynamic viscosity

$$\nu = \frac{\mu}{\rho} \tag{3.26}$$

in case of pure waves U_c in all the above equations is replaced by U_m.

3.6.3 KEULEGAN-CARPENTER NUMBER

For pure waves Keulegan-Carpenter number K_c is given by:

$$K_c = \frac{U_m T}{b} \tag{3.27}$$

where T is the wave period.

4. EXPERIMENTAL SETUP AND PROCEDURE

4.1 EXPERIMENTAL APPARATUS AND EQUIPMENTS

The experiments were conducted in a plexiglass flume. The flume is approximately 23 m long, 0.6 m wide, and 0.7 m deep. A wave paddle is mounted in a deeper section 1 m deep at one end of the flume. There is also an entry tank approximately 4 m long, 2 m wide, and 1.3 m deep which is used as a stilling basin to dampen waves. Currents can be generated using a pump and circulating system. The test section consists of a 4 m long bed of sediment material and 21 cm deep. It was convenient to use concrete blocks for most of the upstream part of the flume to save material as seen in Figure 4.1.

Velocity measurements were taken with a propeller type OTT current meter. This current measuring device is shown in Figure 4.2. The wave generator is an oscillating pendulum type whose stroke and consequently wave height can be varied by adjusting the eccentricity of the paddle arm on the flywheel. The period is controlled by a variable speed drive.

The wave height was measured by a capacitance wave gauge connected to a Hewlett Packard dual channel recorder (Model No. 17501A). Figure 4.3 shows the wave recorder.

4.2 EXPERIMENTAL PROCEUDRE

A total of seventy experiments were conducted for this study. The experiments utilized five cylindrical piles of 1.27, 2.54, 5.08, 8.26, and 11.43 cm in diameter as shown in Figure 4.4.

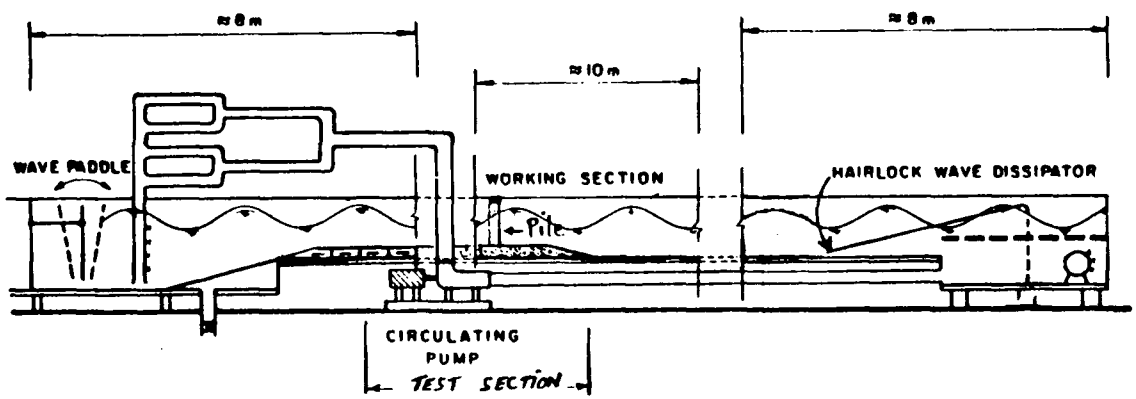

Figure 4.1 Experimental equipment, schematic diagram after Quick (1983).

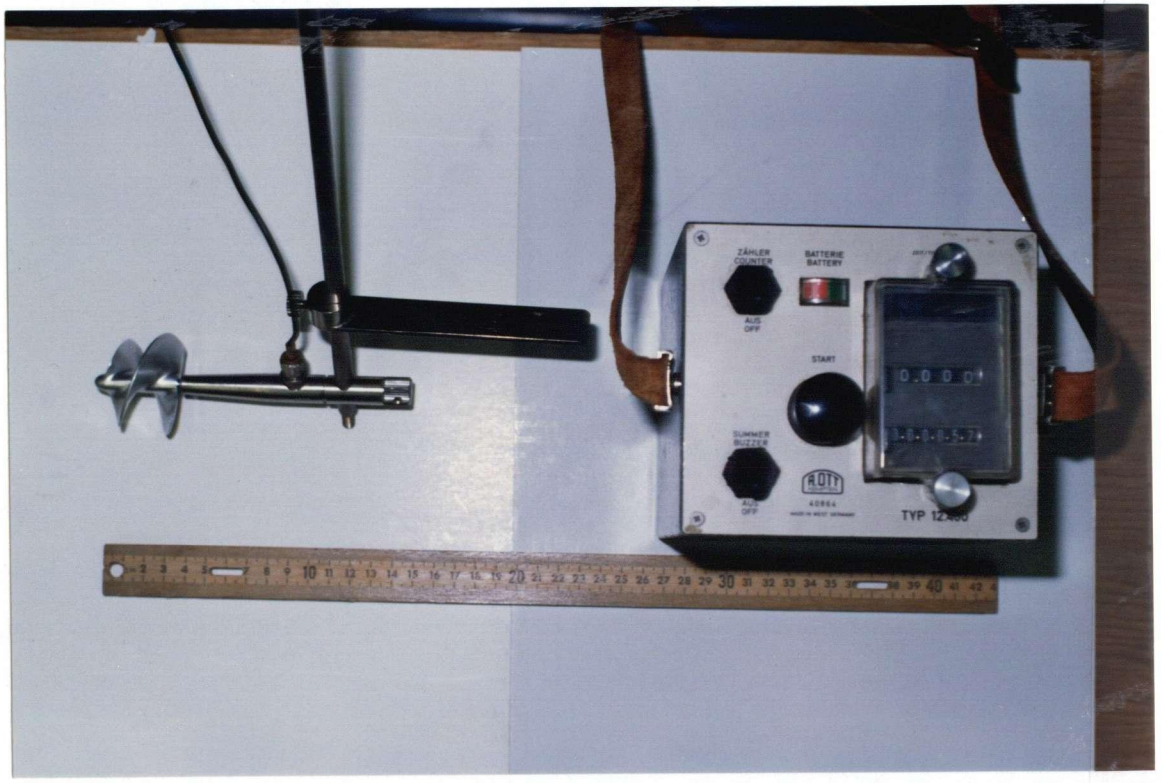

Figure 4.2 OTT current meter.

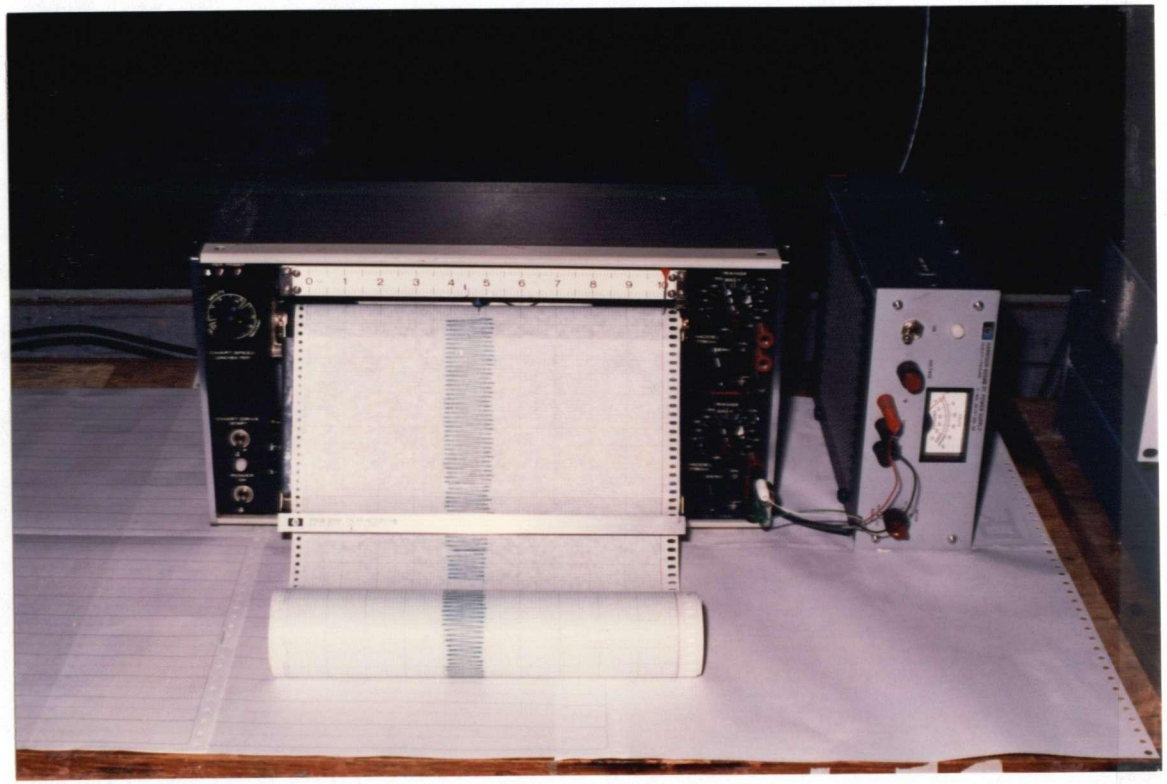

Figure 4.3 Wave recorder.

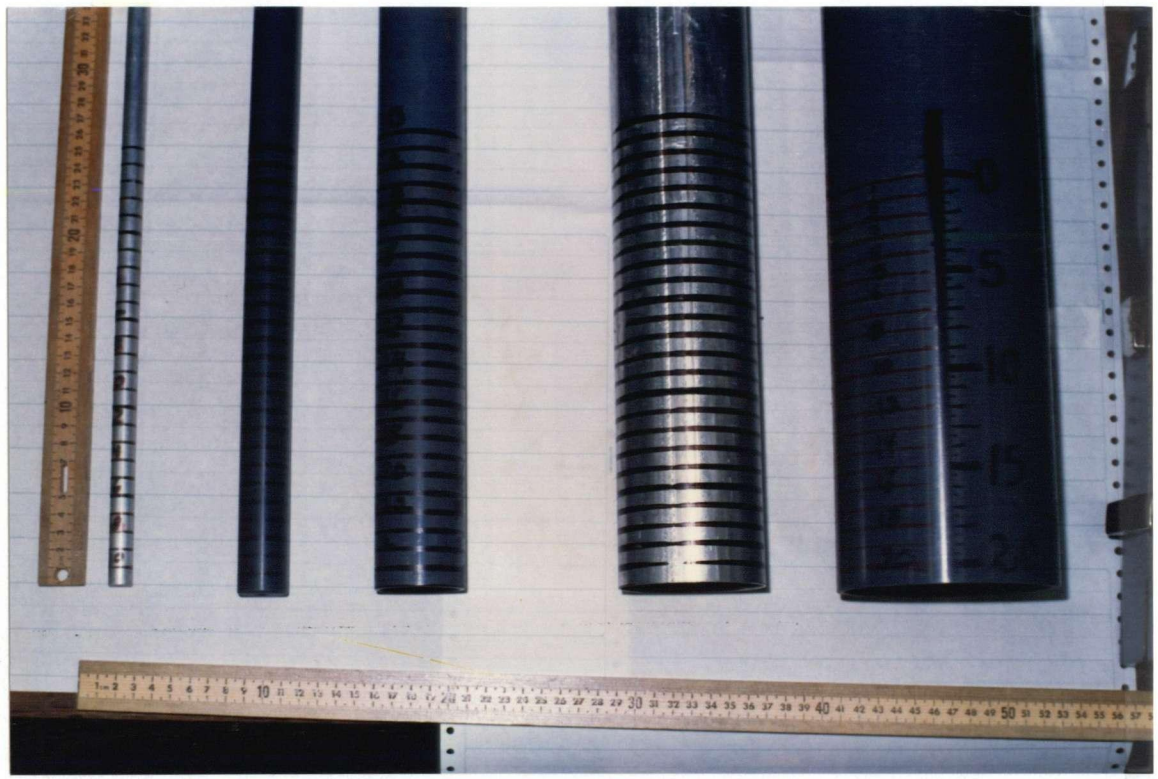

Figure 4.4 Cylindrical Piles.

Sand was the sediment material for this study. These sediments were sieved into a narrow size range so that for a particular experiment onset of sediment motion could be associated with a fairly specific sediment size, these sediment size ranges are 0.3-0.85 mm, 0.85-1.16 mm, and 1.16-1.70 mm. For a particular test series, sediment of certain size was spread uniformly into a flat bed condition. All tests were carried out with the same average water depth of 35 cm. The experiments can be classified into three groups, 15 runs under currents alone, 12 runs with waves alone, and 43 runs under combined waves and currents. For each group of tests the different pile sizes and sediment size ranges were utilized at different flow states, i.e. below, at, and above threshold conditions of each sediment size. For the case of waves alone, the wave period was kept constant at 1.6 seconds and hence the wave length was 2.69 meters. For the case of combined waves and currents, the current velocity is fixed at a certain value and the wave period is adjusted so that the relative wave period is kept the same (1.6 seconds) so that the wave length is unaltered. The wave height and the current velocity were adjusted for each test to the required value.

At the onset of each test, the tank was slowly filled to avoid disturbing the sediment. After a sufficient amount of water had accumulated in the tank, the flow rate through the tank was adjusted to the appropriate setting. The wave generator then started and the period setting and stroke length were adjusted until the desired wave length and wave height were attained. Once this was completed, everything was turned off and the sand bed was relevelled, before the test was started. Scour depth was recorded at various time increments after the test was under way, the increments becoming longer as the test continued. Each

test was conducted until there appeared to be no further increase in scour depth. For the wave-current tests, the experiments ran from 18-26 hours, whereas for the wave only and current alone tests, the running time was less. The maximum scour depth is the maximum depth reached during the test run.

5. PRESENTATION AND DISCUSSION OF RESULTS

A series of tests were performed using different cylinder and sediment sizes, and under different flow conditions in the approaching flow, i.e., below, at, and above threshold of motion. These experiments can be grouped into three sets of tests, currents alone, waves alone, and waves plus currents, and are given the letters C, W, and WC, respectively. Each run in a set was given a number following the set letter, for example, WC12 refers to the run number 12 in the set of combined waves and currents.

The reader should note that both water depth and wave period (hence wave length) are kept constant throughout all the experiments. The aim of the testing was to investigate the ultimate maximum scour which could occur and this was found to be when the approach flow conditions reached critical stress for onset of motion of sediment particles, irregardless of water depth or wave length.

The first set of tests was under the action of currents alone, runs C1 through C15, Table 5.1 from which it can be seen that the maximum scour occurs at threshold conditions in the approaching flow which agrees with the results of Chabert and Engeldinger (1956).

The scour development with time for some of these runs is shown in Figures 5.1 and 5.2 in the form of relative scour (scour depth over cylinder diameter) versus time. These two figures show a decrease in scour depth as the flow conditions in the approaching flow exceed the threshold state which confirms the findings of Chabert and Shen (1966).

In order to check the test results for steady current alone, comparison was made with some well known formulas which already exist.

Run No.	Sediment Size D (mm)	Roughness k_s (mm)	Cylinder Dia. b (cm)	Water Depth d (cm)	Steady Current Velocity U_c (cm/sec)	Max. Scour S (cm)	Relative Scour S/b	F_r	State of Approaching Flow	U_c^* (cm/sec)	Bed Shear τ_o (Pa)	$R_e \times 10^5$
C1	1.16-1.70	1.70	11.43	35	27.48	4.50	0.39	0.148	Below Threshold	0.0153	0.235	0.444
C2	1.16-1.70	1.70	11.43	35	30.28	6.50	0.57	0.163	Below Threshold	0.0169	0.285	0.489
C3	1.16-1.70	1.70	11.43	35	36.44	14.00	1.22	0.197	Below Threshold	0.0203	0.412	0.589
C4	1.16-1.70	1.70	11.43	35	44.60	17.00	1.49	0.241	Below Threshold	0.0249	0.618	0.720
C5	1.16-1.70	1.70	11.43	35	47.73	19.50	1.71	0.258	At Threshold	0.0266	0.708	0.771
C6	1.16-1.70	1.70	11.43	35	53.80	19.00	1.66	0.290	Above Threshold	0.0330	0.899	0.856
C7	1.16-1.70	1.70	11.43	35	59.20	18.50	1.62	0.320	Above Threshold	0.0300	1.100	0.956
C8	1.16-1.70	1.70	2.54	35	41.38	4.25	1.67	0.223	Below Threshold	0.0231	0.532	0.662
C9	1.16-1.70	1.70	2.54	35	47.73	8.10	3.18	0.258	At Threshold	0.0266	0.708	0.771
C10	1.16-1.70	1.70	2.54	35	53.80	6.80	2.68	0.290	Above Threshold	0.0300	0.899	0.869
C11	0.85-1.16	1.16	11.43	35	41.00	22.20	1.94	0.221	At Threshold	0.021	0.460	0.662
C12	0.85-1.16	1.16	8.26	35	41.00	18.10	2.19	0.221	At Threshold	0.021	0.460	0.662
C13	0.85-1.16	1.16	5.08	35	41.00	13.10	2.57	0.221	At Threshold	0.021	0.460	0.662
C14	0.85-1.16	1.16	2.54	35	41.00	9.30	3.66	0.221	At Threshold	0.021	0.460	0.662
C15	0.85-1.16	1.16	1.27	35	41.00	4.80	3.78	0.221	At Threshold	0.021	0.460	0.662

Table 5.1 Experimental results of steady currents alone.

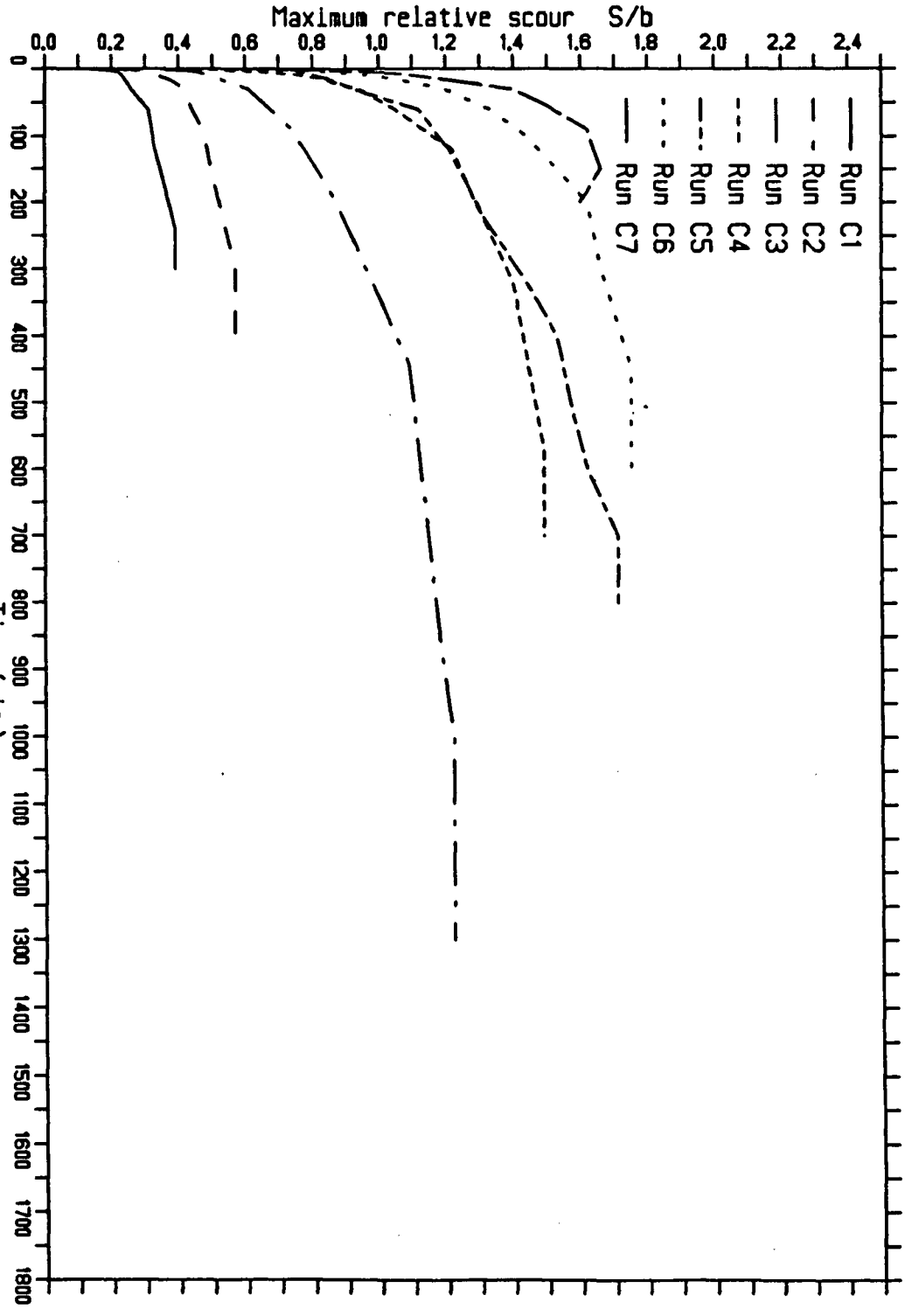

Figure 5.1. Relative scour versus time under steady currents alone.

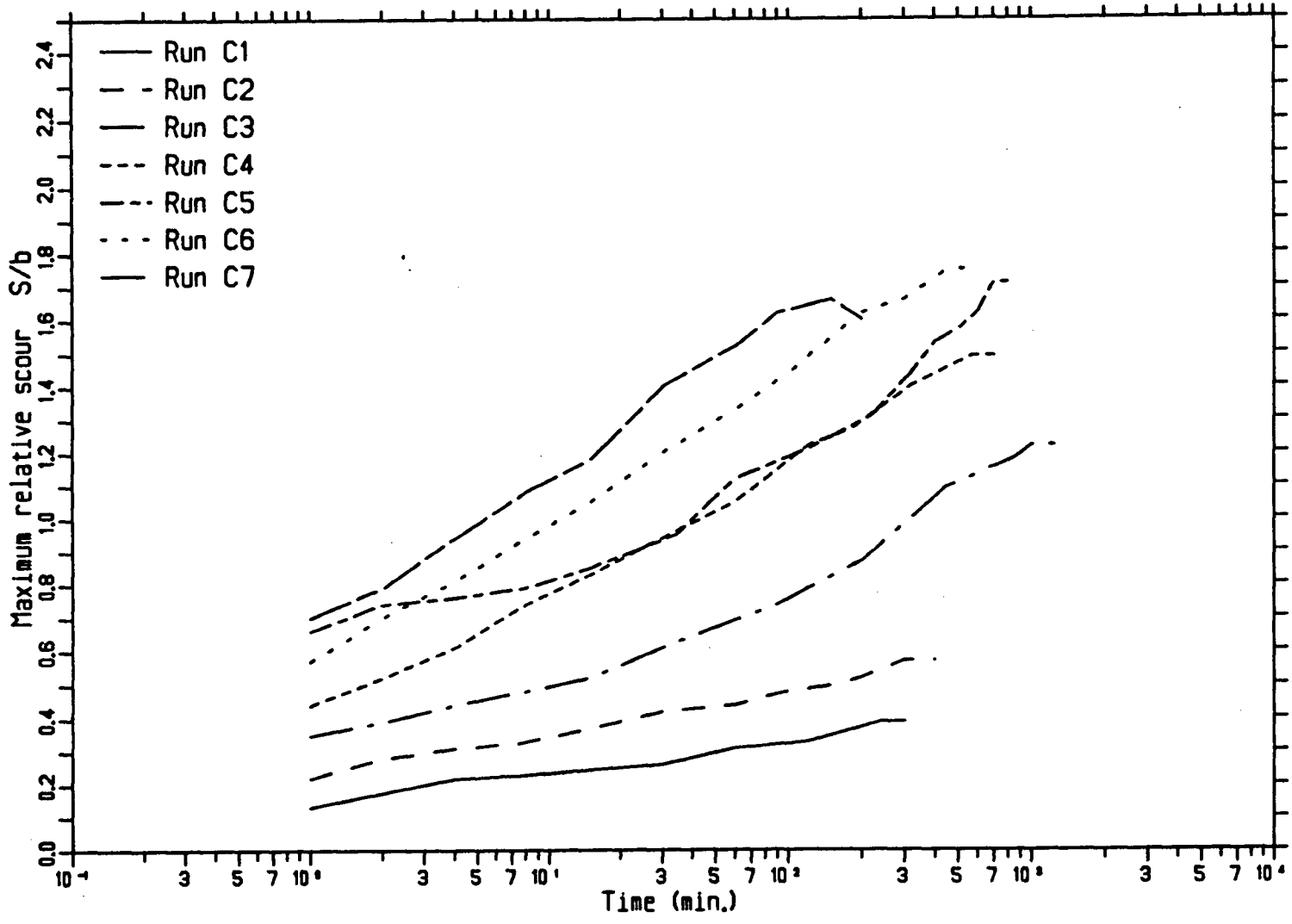

Figure 5.2. Relative scour versus time under steady currents alone.

The comparison is shown in Tables 5.2 through 5.5 for the three sediment sizes tested under threshold conditions and for different cylindrical sizes. It should be noted that the scour depths reported were the maximum possible depths attained during testing. The measured values are in good agreement with most of the estimated values which is another verification for these formulas. Hence it can be argued that steady current scour depths could form a base or a reference for comparison with scour depths under waves or combined waves and currents.

From Table 5.1 it is seen that Froude number F_r is small and less than unity, which makes the flow a subcritical flow. The flow Reynolds number Re is in the order of 10^5, accordingly the flow is fully rough turbulent flow.

The second set of tests was performed under pure waves, runs W1 through W12. The rsults of these runs are presented in Table 5.6, as seen from the table, the depth of scour for the same pile size under the same conditions in the approaching flow is much less than the scour depth under the action of steady currents. The reason for this may be that, although sediment particles are dislodged due to wave turbulence in the vicinity of the cylinder, this turbulence is insufficient to transport the material away because of the reversal flow and the orbital type of horizontal velocity of the wave. The scour development with time is shown in Figures 5.3 and 5.4. Figure 5.5 is a plot of relative scour depth versus pile diameter under the same conditions, from which it can be seen that the relative scour under bigger diameters is less than the relative scour produced by the smaller diameters. It follows that the smaller the K_c, Keulegan-Carpenter number, the bigger is the scour hole depth.

Formula No. / Cyl. Size (cm)	(1.1)	(1.3)	(1.6)	(1.7)	(1.8)	Measured Values
1.27	3.97	3.40	4.39	5.90	4.64	4.80
2.54	6.68	5.39	6.75	9.23	7.53	9.30
5.08	11.24	8.56	10.36	14.44	12.24	13.10
8.26	16.17	11.29	14.06	19.65	17.20	18.10
11.43	20.64	14.69	17.14	22.61	21.59	22.20

Table 5.2 Measured and estimated maximum scour depth S (cm) at threshold conditions in the approaching flow for sediment size range 0.85-1.16mm under steady currents alone.

Formula No. / Cyl. Size (cm)	(1.1)	(1.3)	(1.6)	(1.7)	(1.8)	Measured Values
1.27	3.13	2.67	3.46	4.65	3.65	3.78
2.54	2.36	2.12	2.66	3.63	2.97	3.66
5.08	2.21	1.69	2.04	2.84	2.41	2.57
8.26	1.96	1.43	1.70	2.38	2.08	2.19
11.43	1.81	1.29	1.50	1.99	1.89	1.94

Table 5.3 Measured and estimated maximum relative scour at threshold conditions in the approaching flow for sediment size range 0.85-1.16mm under steady currents alone.

Formula No. / Cyl. Size (cm)	(1.1)	(1.3)	(1.6)	(1.7)	(1.8)	Measured Values
2.54	6.68	7.63	7.42	7.19	7.53	7.50
11.43	20.64	16.26	18.82	18.98	21.59	19.50

Table 5.4 Measured and estimated maximum scour depth in (cm) at threshold conditions in the approaching flow for sediment size range 1.16-1.70mm under steady currents alone.

Formula No. / Cyl. Size (cm)	(1.1)	(1.3)	(1.6)	(1.7)	(1.8)	Measured Values
2.54	2.63	3.01	3.00	2.83	2.97	2.95
11.43	1.81	1.42	1.65	1.66	1.89	1.71

Table 5.5 Measured and estimated maximum relative scour at threshold conditions in the approaching flow for sediment size range 1.16-1.70mm under steady currents alone.

Run No.	Sediment Size D (mm)	k_s (mm)	Cylinder Dia. b (cm)	State of Approaching Flow	Max. Scour S (cm)	Relative Maximum Scour S/b	H (cm)	U_w (cm/s)	a_{1m} (cm)	$R_e \times 10^5$	K_c
W3	1.16-1.70	1.70	11.43	At Threshold	2.30	0.20	13.00	31.96	7.13	0.288	4.47
W4	1.16-1.70	1.70	11.43	Above Threshold	1.68	0.51	14.60	36.47	8.01	0.292	5.11
W5	1.16-1.70	1.70	2.54	Below Threshold	1.80	0.71	10.50	25.17	5.76	0.145	15.86
W6	1.16-1.70	1.70	2.54	At Threshold	3.10	1.22	13.00	31.96	7.13	0.288	20.13
W7	1.16-1.70	1.70	2.54	Above Threshold	3.00	1.18	14.00	34.76	7.70	0.267	21.90
W8	0.85-1.16	1.16	11.43	At Threshold	4.50	0.39	11.80	28.70	6.50	0.187	4.02
W9	0.85-1.16	1.16	8.26	At Threshold	4.50	0.53	11.80	28.70	6.50	0.187	5.56
W10	0.85-1.16	1.16	5.08	At Threshold	4.30	0.84	11.80	28.70	6.50	0.187	9.04
W11	0.85-1.16	1.16	2.54	At Threshold	3.70	1.46	11.80	28.70	6.50	0.187	18.08
W12	0.85-1.16	1.16	1.27	At Threshold	3.50	2.80	11.80	28.70	6.50	0.187	36.16

Table 5.6 Experimental results of oscillatory waves alone.

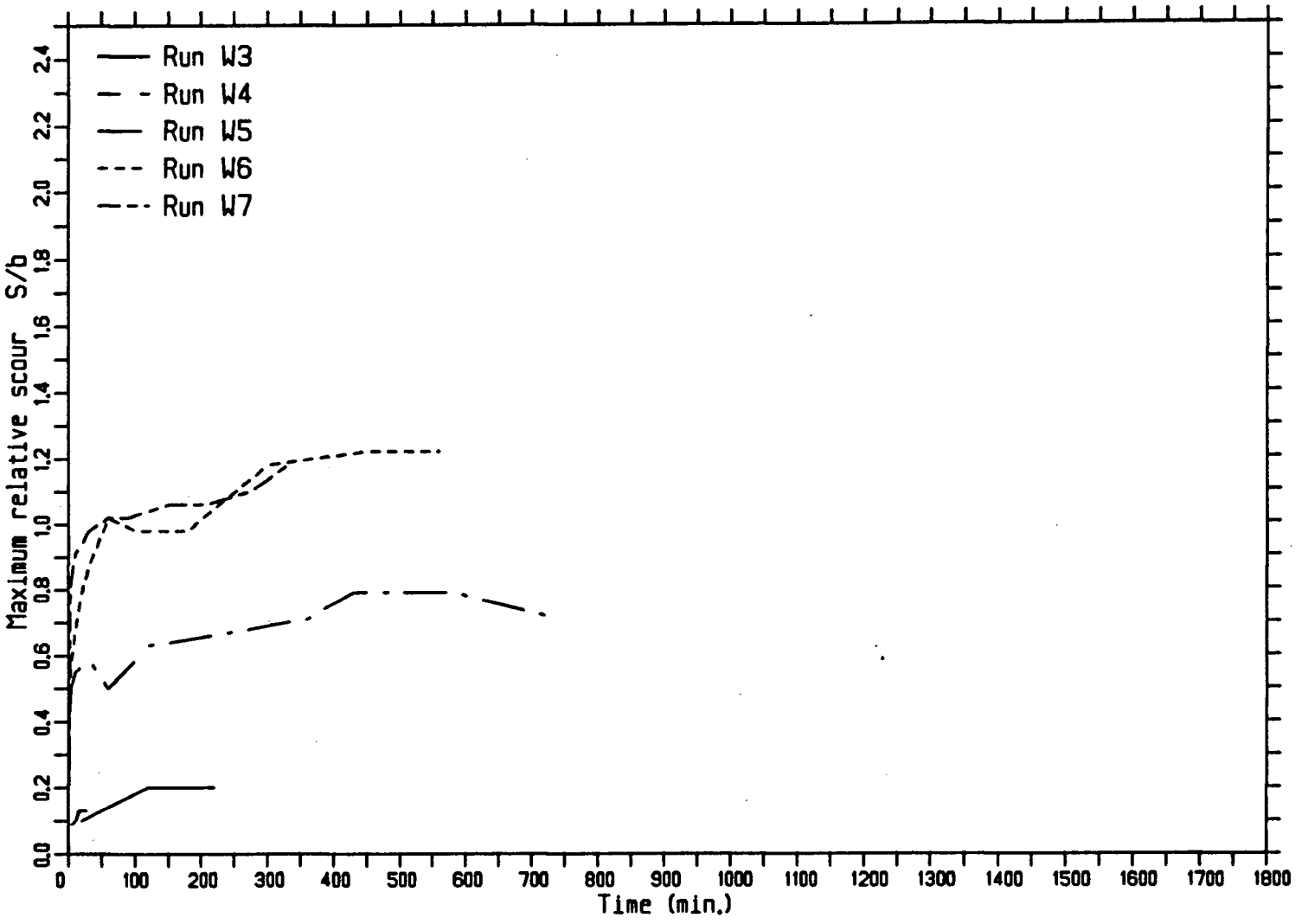

Figure 5.3. Relative scour versus time under pure waves.

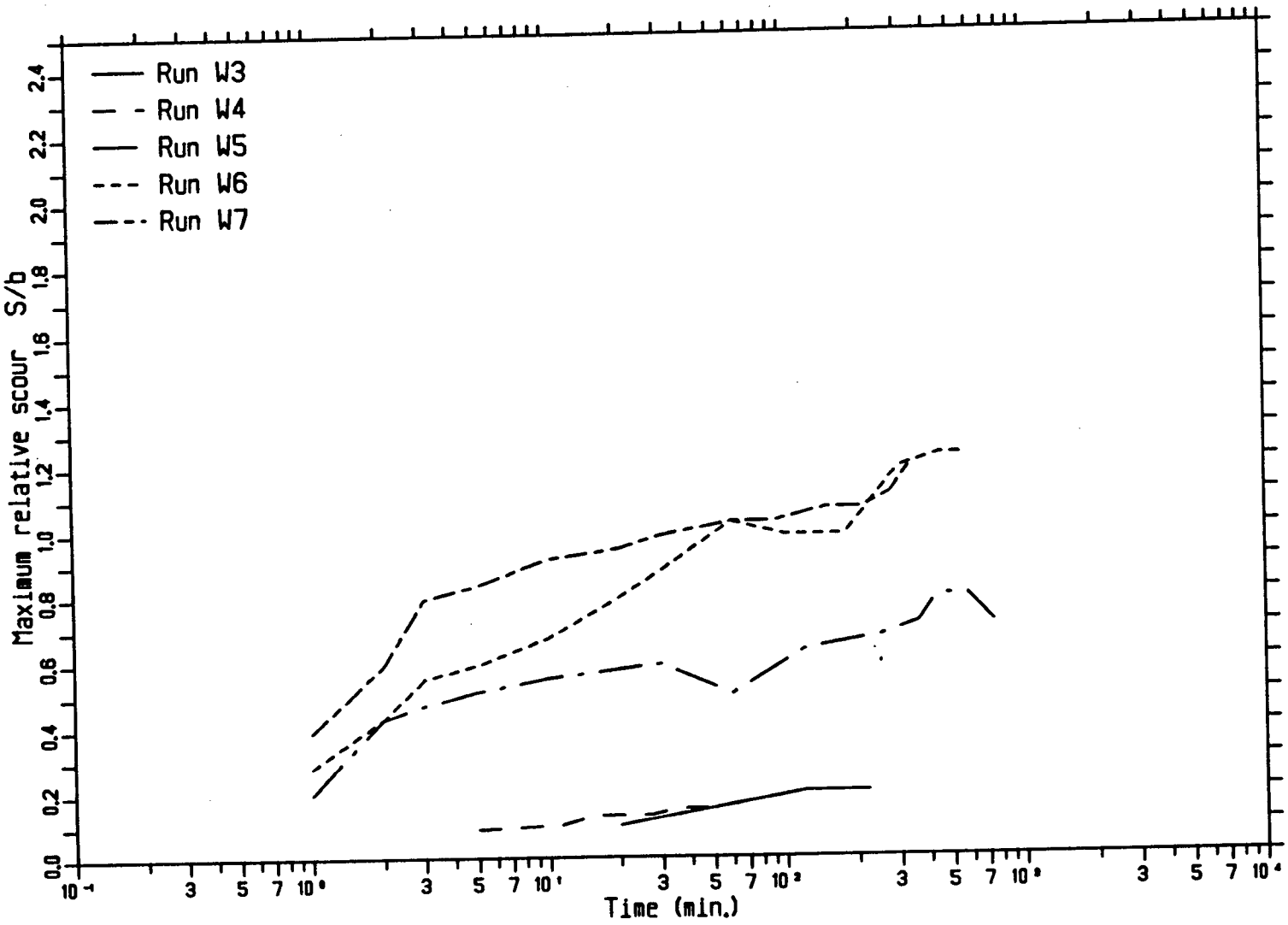

Figure 5.4. Relative scour versus time under pure waves.

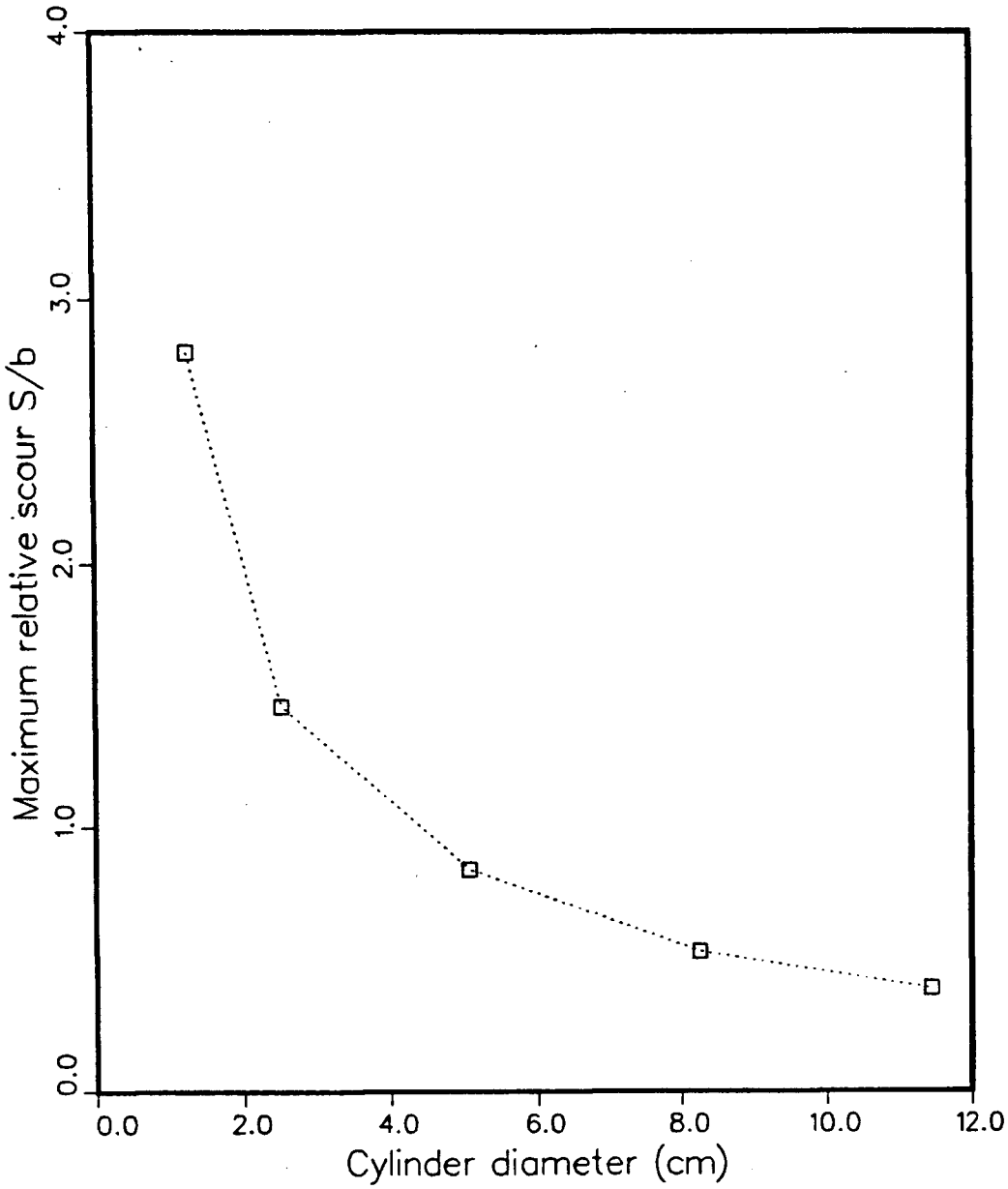

Figure 5.5. Maximum relative scour versus cylinder diameter for Oscillatory flow at threshold conditions; sediment size 0.85-1.16 mm.

Further series of tests were carried out to investigate how scour is produced under the action of combined waves and currents. In particular, the conditions were investigated which produce the maximum scour depth.

This third set of tests under the combined waves and currents was labelled runs WC1 through WC43, and the results are tabulated in Table 5.7.

Relative maximum scour versus time plots are shown in Figures 5.6 and 5.7, both of them show a development with time similar to that of unidirectional flows (see Figures 5.1 and 5.2).

Referring to Table 5.7, it can be seen that runs WC3 and WC6 are under similar sediment threshold conditions, but the resulting scour depths are different, and the same is true for runs WC9 and WC11. This difference in scour depth can be explained because, although a threshold state condition was attained for all the runs, the contribution of the waves and currents to the critical velocity at bed in each case is different. For example in run WC3 the wave height was 10.5 cm and the steady current velocity was 23 cm/sec, whereas in run WC6 the wave height was 9.4 and the steady current velocity was 30.28 cm/sec, for both of the runs the maximum velocity at bed due to combined wave and current was 32.8 cm/sec.

From the first few tests a conclusion was reached, that maximum scour depths under combined waves and currents occurred when threshold sediment conditions existed in the approaching flow, and therefore most of the rest of this set was performed under this threshold condition. An attempt was made to investigate the influence on scour of flow parameters, such as cylinder size, sediment size, and the proportion of wave motion to current velocity. Runs WC29 through WC43, C11 through

Run No.	Sediment Size D (mm)	k_s (mm)	Cylinder Dia. b (cm)	State of Approaching Flow	Max. Scour S (cm)	Maximum Relative Scour S/b	U_c (cm/sec)	H (cm)	U_w (cm/s)	U_{wc} (cm/s)	Equiv. U^*_{wc} (cm/sec)	τ_{wc} Pa
WC1	1.16-1.70	1.70	11.43	Below Threshold	8.00	0.70	23.00	6.00	13.72	24.00	2.08	0.434
WC2	1.16-1.70	1.70	11.43	Below Threshold	10.70	0.94	23.00	8.50	19.96	30.24	2.61	0.683
WC3	1.16-1.70	1.70	11.43	At Threshold	15.00	1.31	23.00	10.50	25.17	32.80	2.85	0.814
WC4	1.16-1.70	1.70	11.43	Above Threshold	14.00	1.42	23.00	12.00	29.21	40.00	3.48	1.210
WC5	1.16-1.70	1.70	11.43	Below Threshold	16.20	1.51	30.28	7.20	16.68	31.04	2.70	0.729
WC6	1.16-1.70	1.70	11.43	At Threshold	17.30	1.40	30.28	9.40	22.80	32.80	2.85	0.814
WC7	1.16-1.70	1.70	11.43	Above Threshold	16.00	1.22	30.28	11.80	28.66	43.03	3.74	1.400
WC8	1.16-1.70	1.70	2.54	Below Threshold	5.00	1.97	27.76	7.50	17.43	30.60	2.66	0.708
WC9	1.16-1.70	1.70	2.54	At Threshold	5.00	1.97	27.76	9.40	22.30	32.80	2.85	1.040
WC10	1.16-1.70	1.70	2.54	Above Threshold	5.00	1.97	27.76	10.00	23.85	37.00	3.22	0.814
WC11	1.16-1.70	1.70	2.54	At Threshold	3.50	1.38	13.70	10.50	25.17	32.80	2.85	0.814
WC12	1.16-1.70	1.70	2.54	At Threshold	5.00	1.97	22.30	9.10	21.50	32.80	2.85	0.814
WC13	1.16-1.70	1.70	2.54	Below Threshold	7.10	2.80	31.12	6.50	14.95	32.80	2.85	0.814
WC14	1.16-1.70	1.70	11.43	At Threshold	17.40	1.52	31.12	6.40	14.70	32.80	2.85	0.814
WC15	1.16-1.70	1.70	1.27	At Threshold	4.00	3.14	31.12	7.70	17.93	32.80	2.85	0.814

Table 5.7. Experimental results of combined waves and currents.

Run No.	Sediment Size D (mm)	k_s (mm)	Cylinder Dia. b (cm)	State of Approaching Flow	Max. Scour S (cm)	Maximum Relative Scour S/b	U_c (cm/sec)	H (cm)	U_w (cm/s)	U_{wc} (cm/s)	Equiv. U^*_{wc} (cm/sec)	τ_{wc} Pa
WC16	1.16-1.70	1.70	2.54	At Threshold	7.10	2.80	31.12	7.70	17.93	32.80	2.85	0.814
WC17	1.16-1.70	1.70	5.08	At Threshold	10.50	2.10	31.12	7.70	17.93	32.80	2.85	0.814
WC18	1.16-1.70	1.70	8.26	At Threshold	15.50	1.88	31.12	7.70	17.93	32.80	2.85	0.814
WC19	0.85-1.16	1.16	1.27	At Threshold	4.50	3.54	31.12	6.80	15.68	29.50	2.57	0.658
WC20	0.85-1.16	1.16	2.54	At Threshold	8.00	3.51	31.12	6.80	15.68	29.50	2.57	0.658
WC21	0.85-1.16	1.16	5.08	At Threshold	11.00	2.17	31.12	6.80	15.68	29.50	2.57	0.658
WC22	0.85-1.16	1.16	8.26	At Threshold	16.20	1.96	31.12	6.80	15.68	29.50	2.57	0.658
WC23	0.85-1.16	1.16	11.43	At Threshold	18.30	1.60	31.12	6.80	15.68	29.50	2.57	0.658
WC24	0.30-0.85	0.85	11.43	At Threshold	5.00	3.94	28.60	6.75	15.56	27.60	2.40	0.576
WC25	0.30-0.08	0.85	2.54	At Threshold	8.50	3.35	28.60	6.75	15.56	27.60	2.40	0.576
WC26	0.30-0.08	0.85	5.08	At Threshold	11.80	2.32	28.60	6.75	15.56	27.60	2.40	0.576
WC27	0.30-0.08	0.85	8.26	At Threshold	17.00	2.10	28.60	6.75	15.56	27.60	2.40	0.576
WC28	0.30-0.08	0.85	11.43	At Threshold	19.20	1.66	28.60	6.75	15.56	27.60	2.40	0.576
WC29	0.85-1.16	1.16	11.43	At Threshold	19.30	1.69	34.20	3.50	7.60	29.50	2.57	0.658
WC30	0.85-1.16	1.16	8.26	At Threshold	15.20	1.84	34.20	3.50	7.60	29.50	2.57	0.658

Table 5.7. Continued

Run No.	Sediment Size D (mm)	k_s (mm)	Cylinder Dia. b (cm)	State of Approaching Flow	Max. Scour S (cm)	Maximum Relative Scour S/b	U_c (cm/sec)	H (cm)	U_w (cm/s)	U_{wc} (cm/s)	Equiv. U^*_{wc} (cm/sec)	τ_{wc} Pa
WC31	0.85-1.16	1.16	5.08	At Threshold	11.10	2.20	34.20	3.50	7.60	29.50	2.57	0.658
WC32	0.85-1.16	1.16	2.54	At Threshold	7.20	2.83	34.20	3.50	7.60	29.50	2.57	0.658
WC33	0.85-1.16	1.16	1.27	At Threshold	4.10	3.30	34.20	3.50	7.60	29.50	2.57	0.658
WC34	0.85-1.16	1.16	11.43	At Threshold	14.50	1.27	28.60	6.00	13.70	29.50	2.57	0.658
WC35	0.85-1.16	1.16	8.26	At Threshold	10.30	1.25	28.60	6.00	13.70	29.50	2.57	0.658
WC36	0.85-1.16	1.16	5.08	At Threshold	8.50	1.67	28.60	6.00	13.70	29.50	2.57	0.658
WC37	0.85-1.16	1.16	2.54	At Threshold	5.90	2.30	28.60	6.00	13.70	29.50	2.57	0.658
WC38	0.85-1.16	1.16	1.27	At Threshold	4.00	3.15	28.60	6.00	13.70	29.50	2.57	0.658
WC39	0.85-1.16	1.16	11.43	At Threshold	9.80	0.86	17.40	9.00	21.20	29.50	2.57	0.658
WC40	0.85-1.16	1.16	8.26	At Threshold	8.10	0.98	17.40	9.00	21.20	29.50	2.57	0.658
WC41	0.85-1.16	1.16	5.08	At Threshold	5.80	1.14	17.40	9.00	21.20	29.50	2.57	0.658
WC42	0.85-1.16	1.16	2.54	At Threshold	4.70	1.85	17.40	9.00	21.20	29.50	2.57	0.658
WC43	0.85-1.16	1.16	1.27	At Threshold	3.70	2.90	17.40	9.00	21.20	29.50	2.57	0.658

Table 5.7. Continued

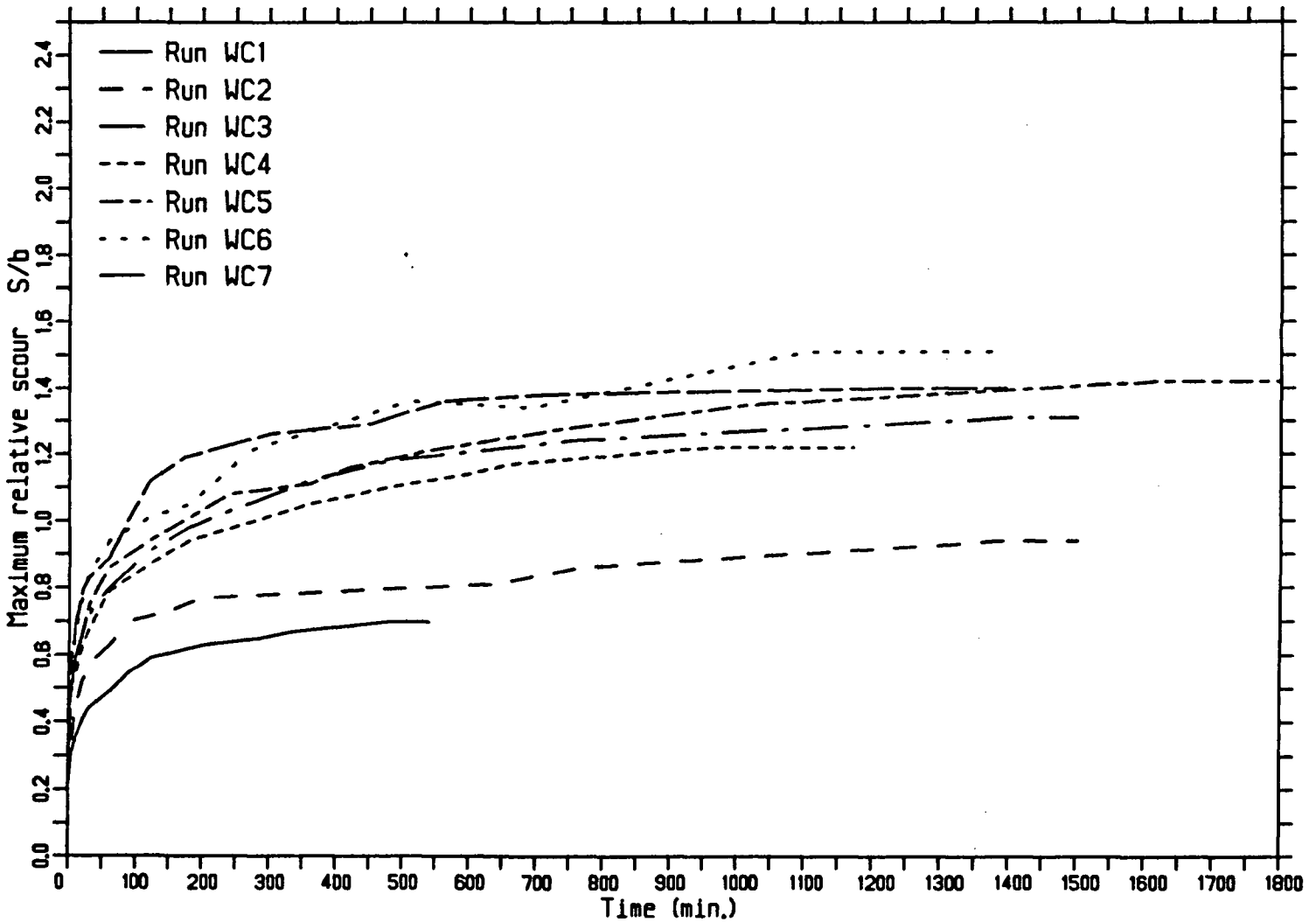

Figure 5.6. Relative scour versus time under combined waves and currents.

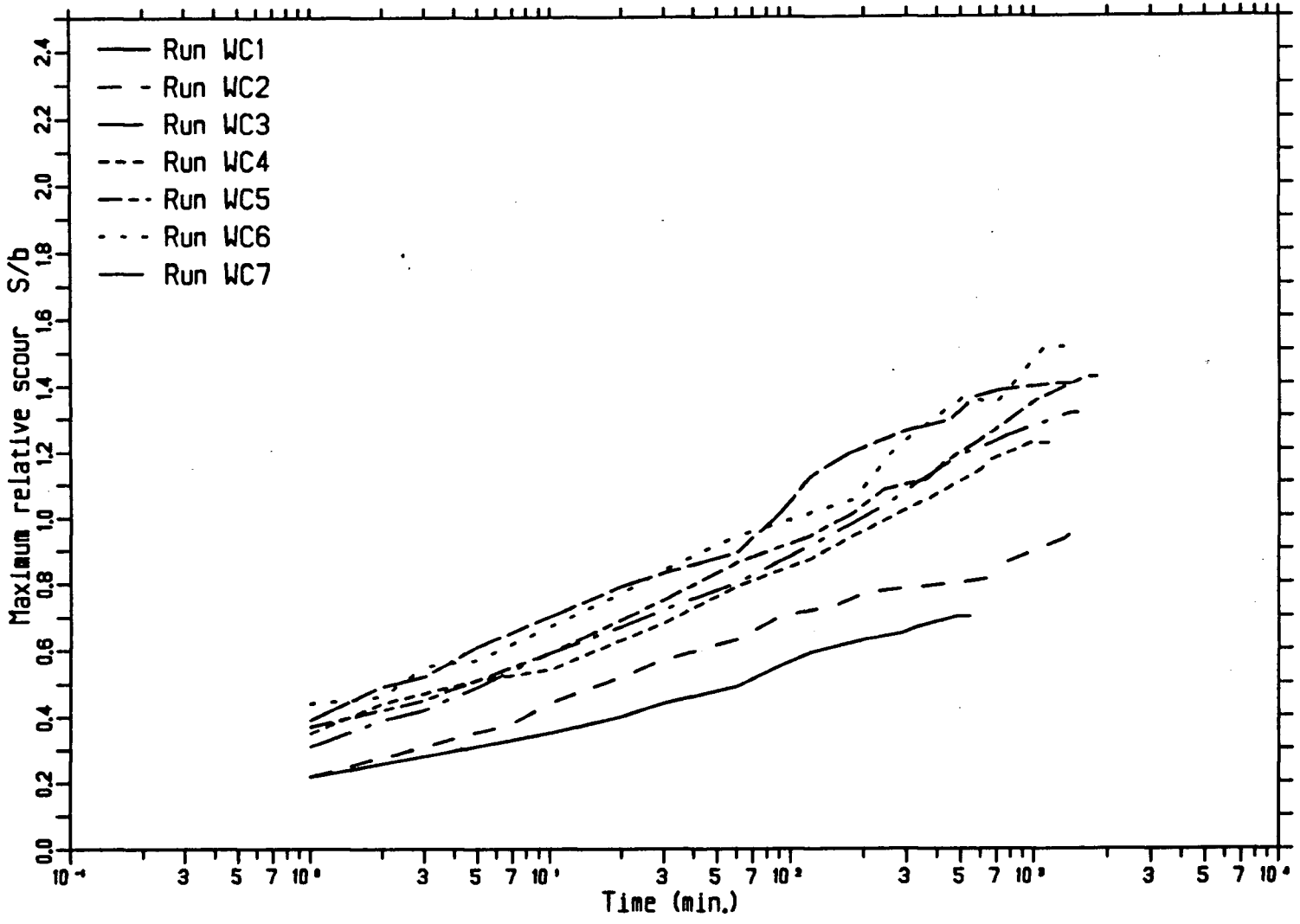

Figure 5.7. Relative scour versus time under combined waves and currents.

C15, and W8 through W12 were at threshold conditions for a sediment size range of 0.85-1.16 mm using the five cylinder sizes. These runs can be divided into five groups as seen in Table 5.8 according to the contribution of both the wave and current flow components to the total critical velocity at the bed.

Run No.	Percentage of Wave in Threshold Velocity (%)	Percentage of Current in Threshold Velocity (%)
C11 - C15	0	100
WC29 - WC33	25	75
WC34 - WC39	50	50
WC39 - WC43	75	25
W8 - W12	100	0

Table 5.8 Contribution of waves and currents in threshold velocity (%)

The results of these tests are presented in Figures 5.8 through 5.11, each plot contains five curves, a curve for each cylinder size. The plot of the wave percentage in the threshold velocity of the combined wave and current versus the maximum scour is shown in Figure 5.8 and versus the maximum relative scour is shown in Figure 5.9.

For threshold or critical velocity for onset of motion in the approach flow, Figure 5.8 shows that the maximum scour depth is varying almost linearly according to the contribution of both waves and currents. It also shows that the more is the current percentage in the critical combined flow velocity, the more is the scour depth. At the limit, scour reaches the steady current value and this is true for all the cylinder sizes tested. It should be noted that larger cylinder sizes are more sensitive to changes in the critical flow velocity than for the smaller sizes.

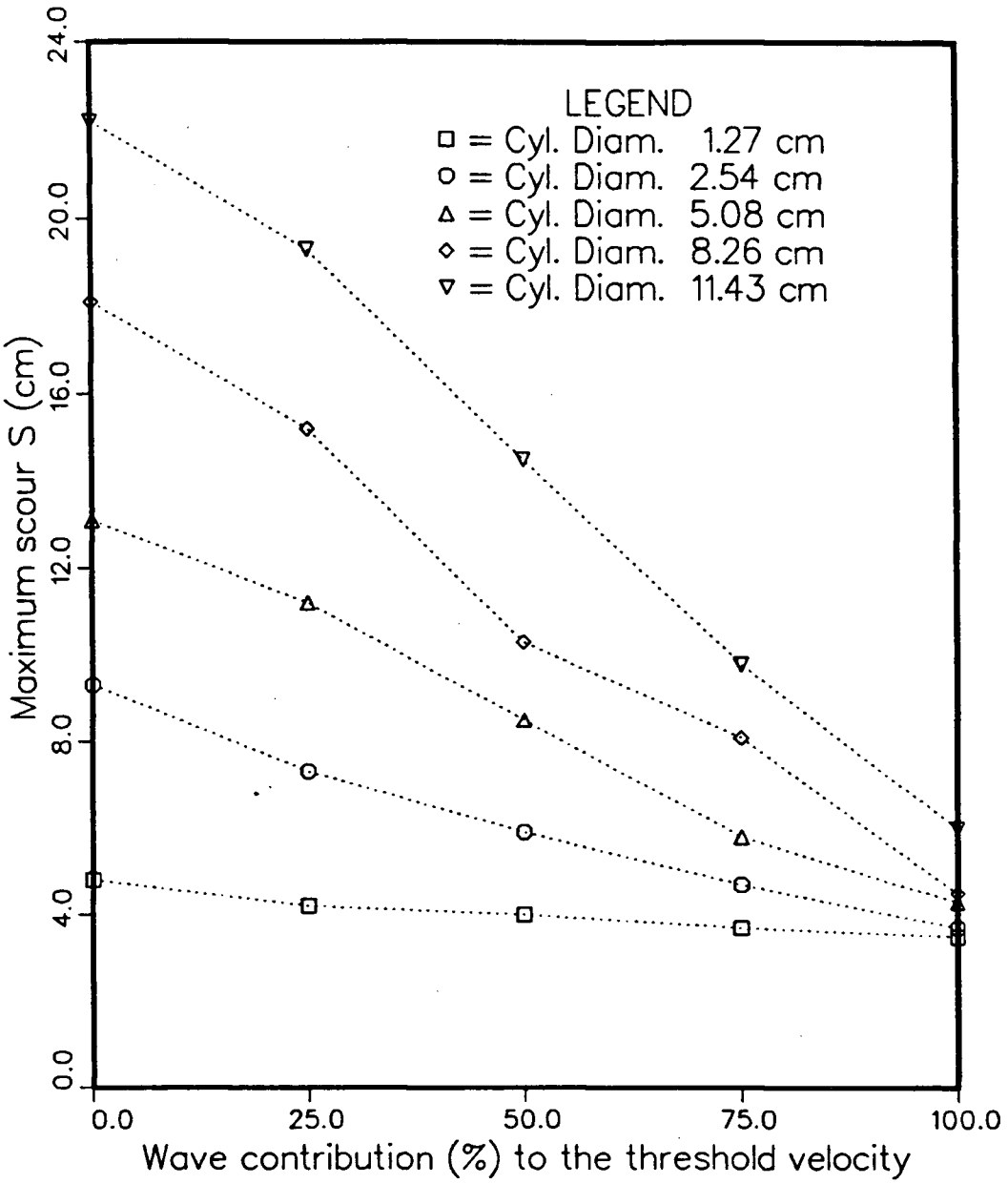

Figure 5.8. Maximum scour versus combined waves and current threshold velocity, sediment size 0.30 - 0.85.

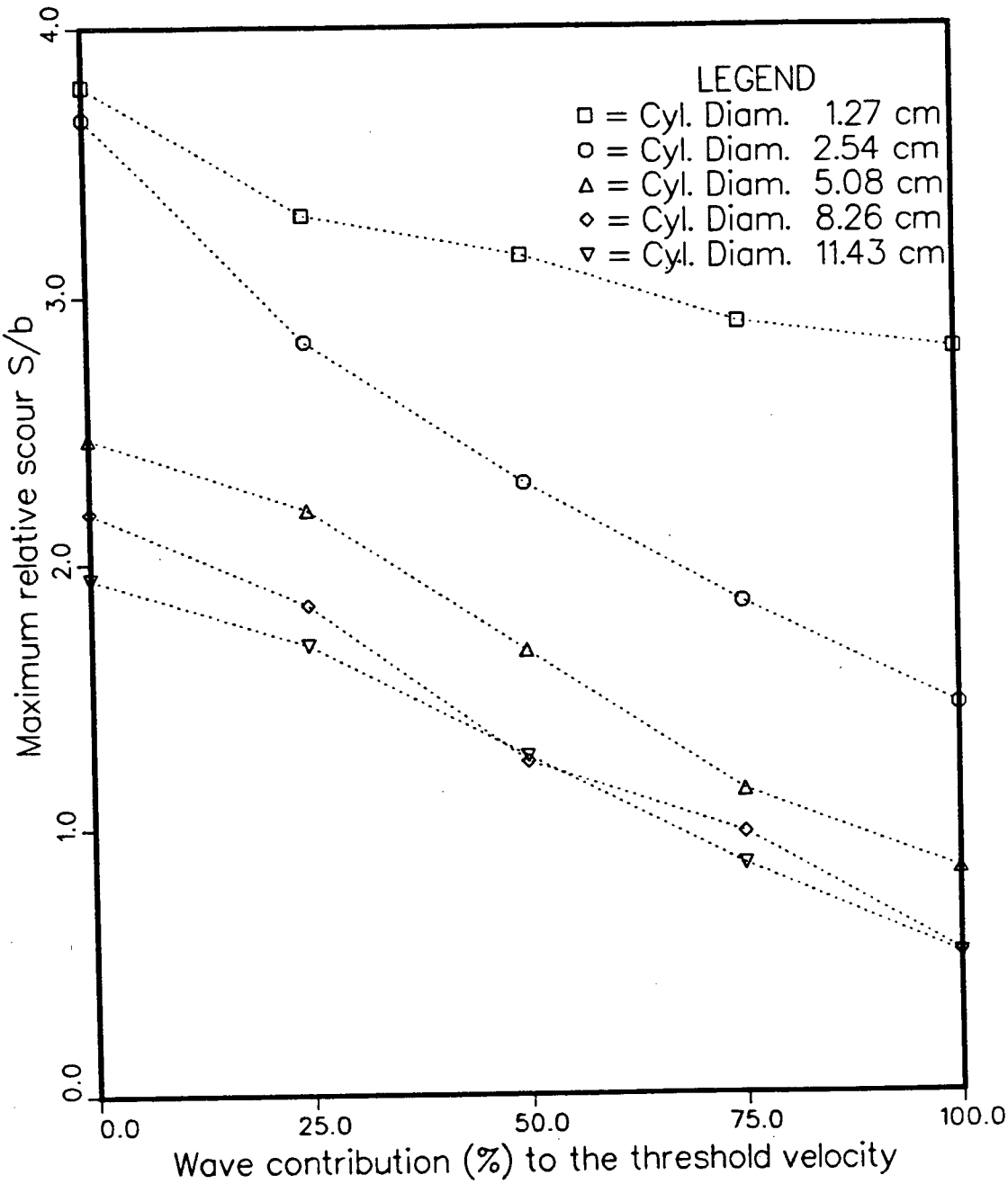

Figure 5.9. Maximum relative scour versus combined waves and currents threshold velocity; sediment size 0.30 - 0.85 mm.

Figure 5.10 shows the change of maximum scour depth with respect to the cylinder size for different flow combinations. In this figure the scour depth under the action of pure currents increases considerably as the cylinder size increases, while for pure waves the change in scour depth as the cylinder size varies is not very great.

Figure 5.11 shows that maximum relative scour for smaller cylinder sizes is greater than the relative scour of bigger diameters, and this is valid for the different flow cases tested.

Figure 5.12 and 5.13 show scour results when contributions to threshold conditions are 25% waves and 75% current. The maximum scour depth is plotted against cylinder diameter for the three sediment size ranges tested. Although the change is not so high, the smaller sediment size ranges are scoured more than the bigger sediment sizes.

From the visual observations it was found that the pattern of the scour hole is very similar for all the flow cases tested; for most of the tests the maximum scour depth was at the front of the pile facing the upstream side of the flow. A typical scour hole under combined wave and current is shown in Figures 5.14 and 5.15. It was noted that the scour around the cylinder under the combination of waves and currents takes place because sediment particles are dislodged or entrained by the wave and the current turbulence and then transported by the flow current.

The scour mechanism under the action of combined waves and currents seems to be similar to the mechanism under currents or waves alone. Erosion is restricted to a narrow width adjacent to the pile and at the bottom of the scour hole. The rest of scour hole is at the angle of repose and material slumps into the hole as the scour proceeds. For the

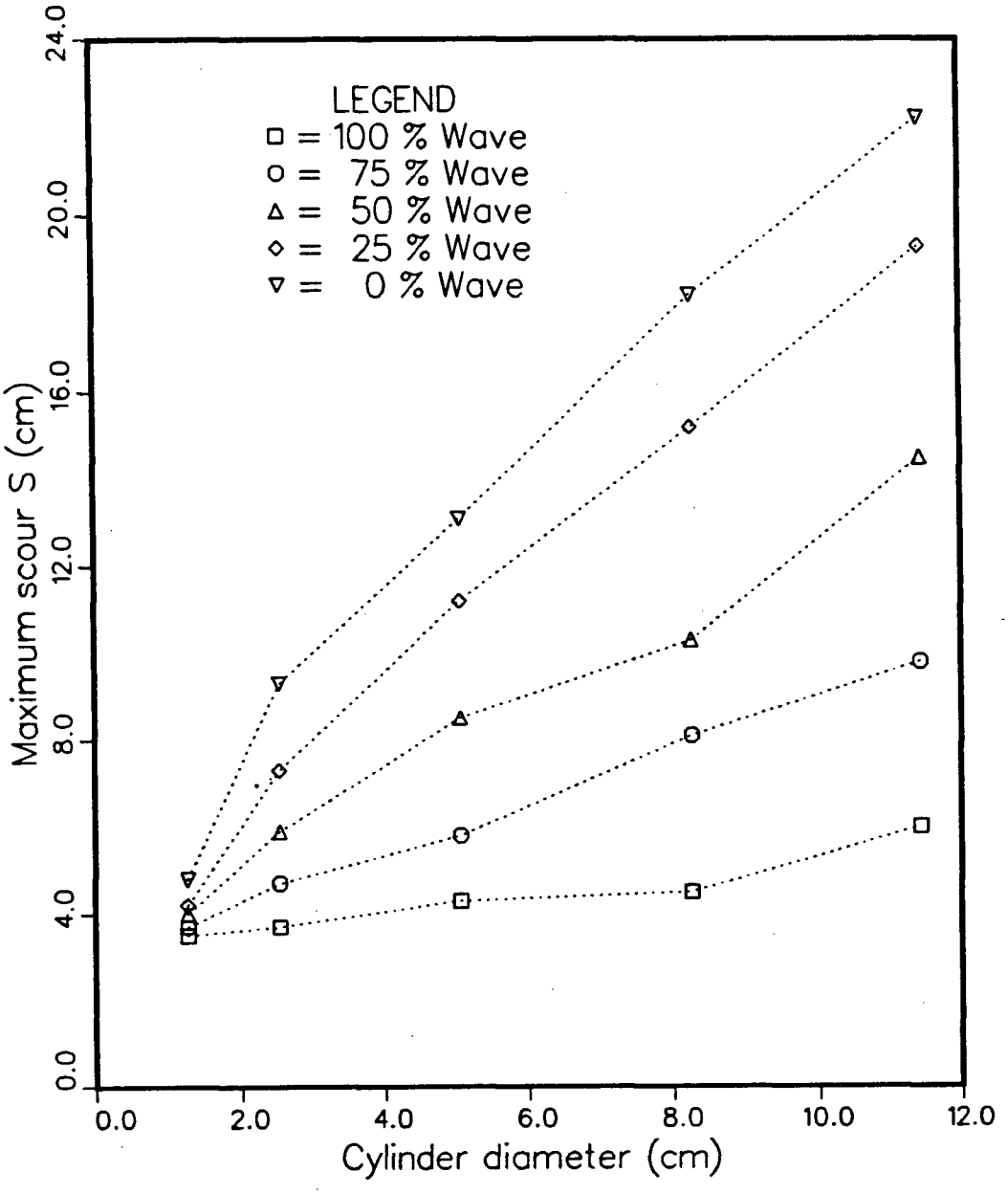

Figure 5.10. Maximum scour versus cylinder diameter at threshold conditions of combined waves and currents; sediment size 0.3 - 0.85 mm.

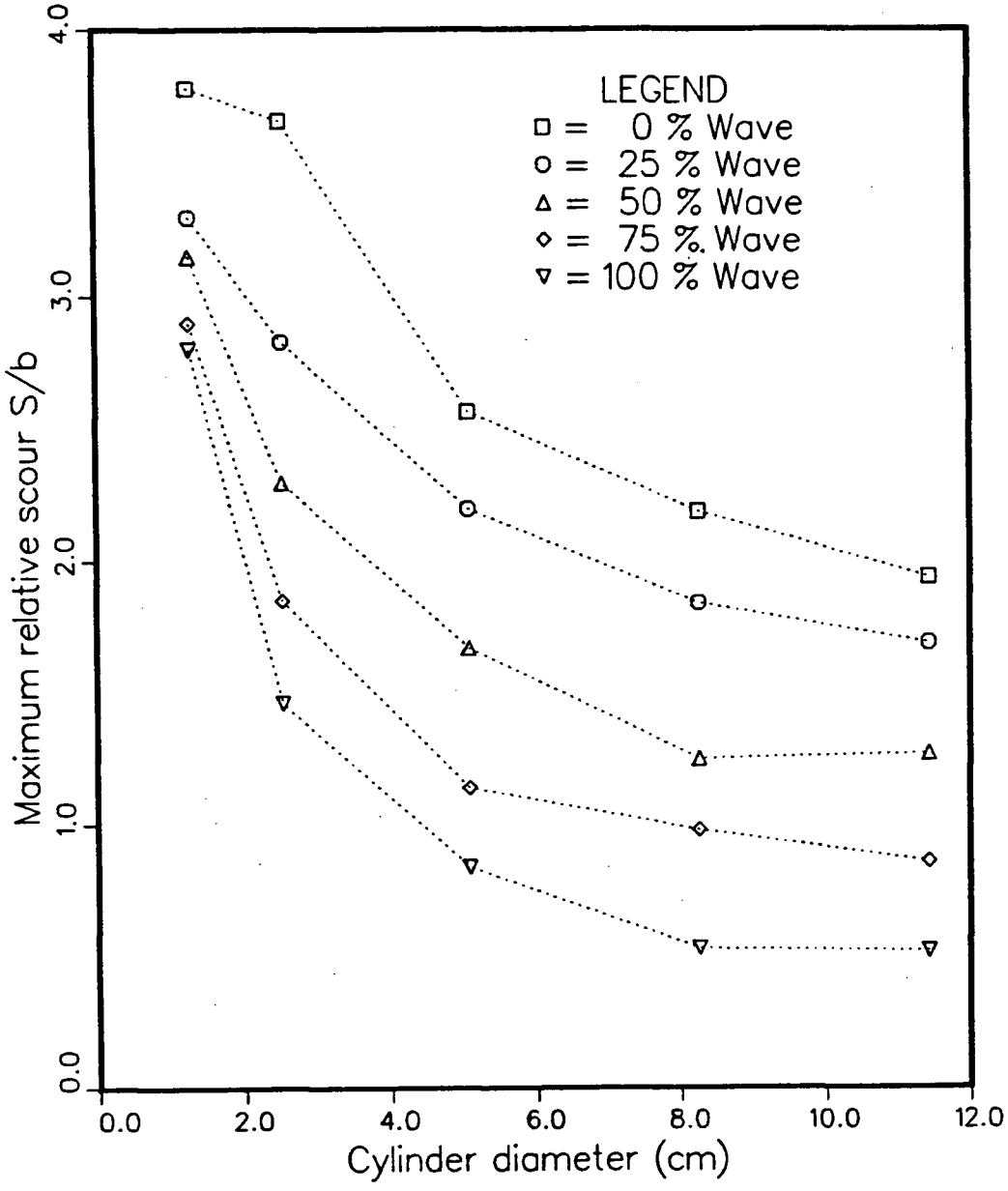

Figure 5.11. Maximum relative scour versus cylinder diameter at threshold conditions of combined waves and currents; sediment size 0.3 - 0.85 mm.

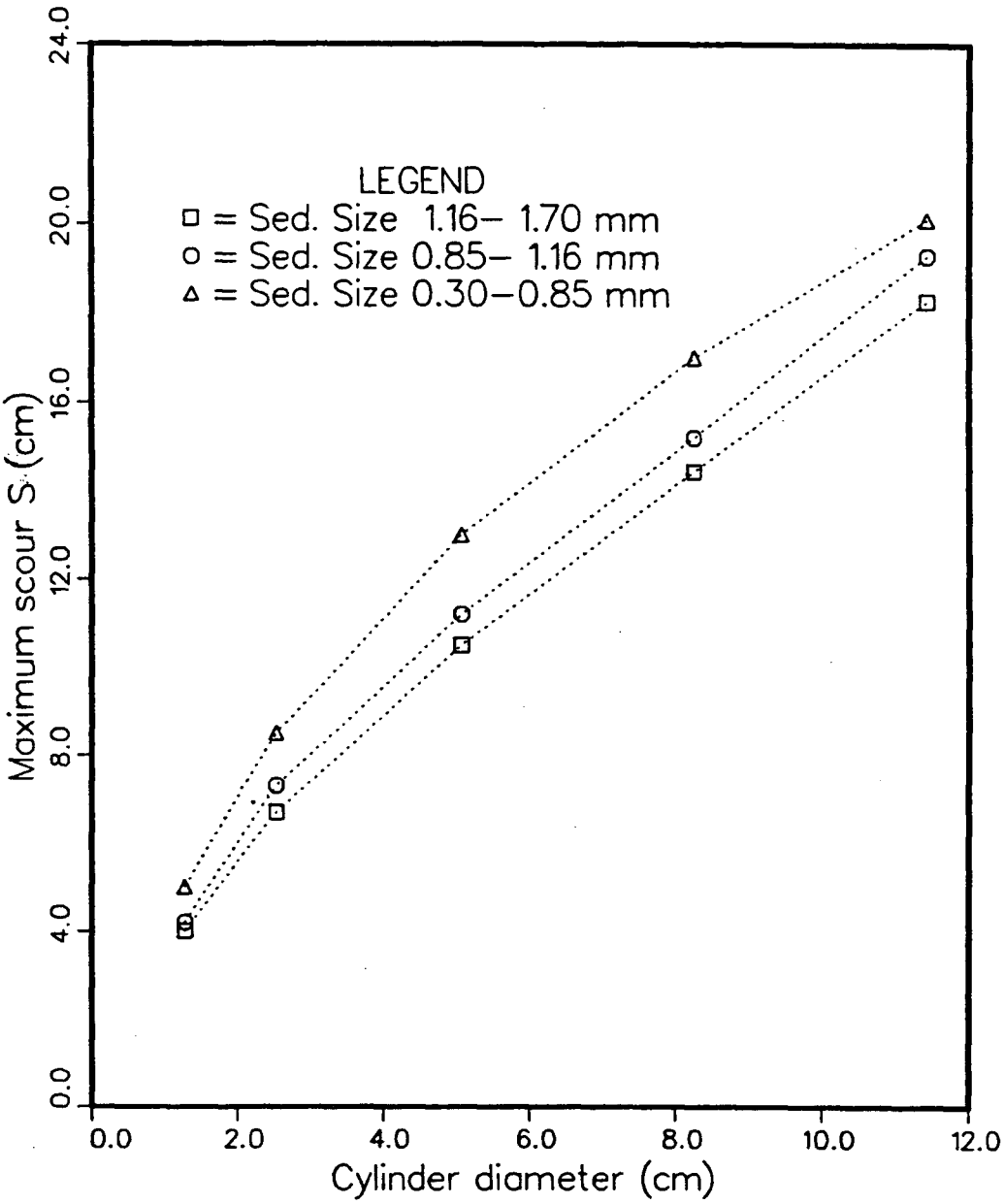

Figure 5.12. Maximum scour depth versus cylinder diameter for three sediment sizes under threshold conditions of combined waves and currents; 25% wave and 75% current.

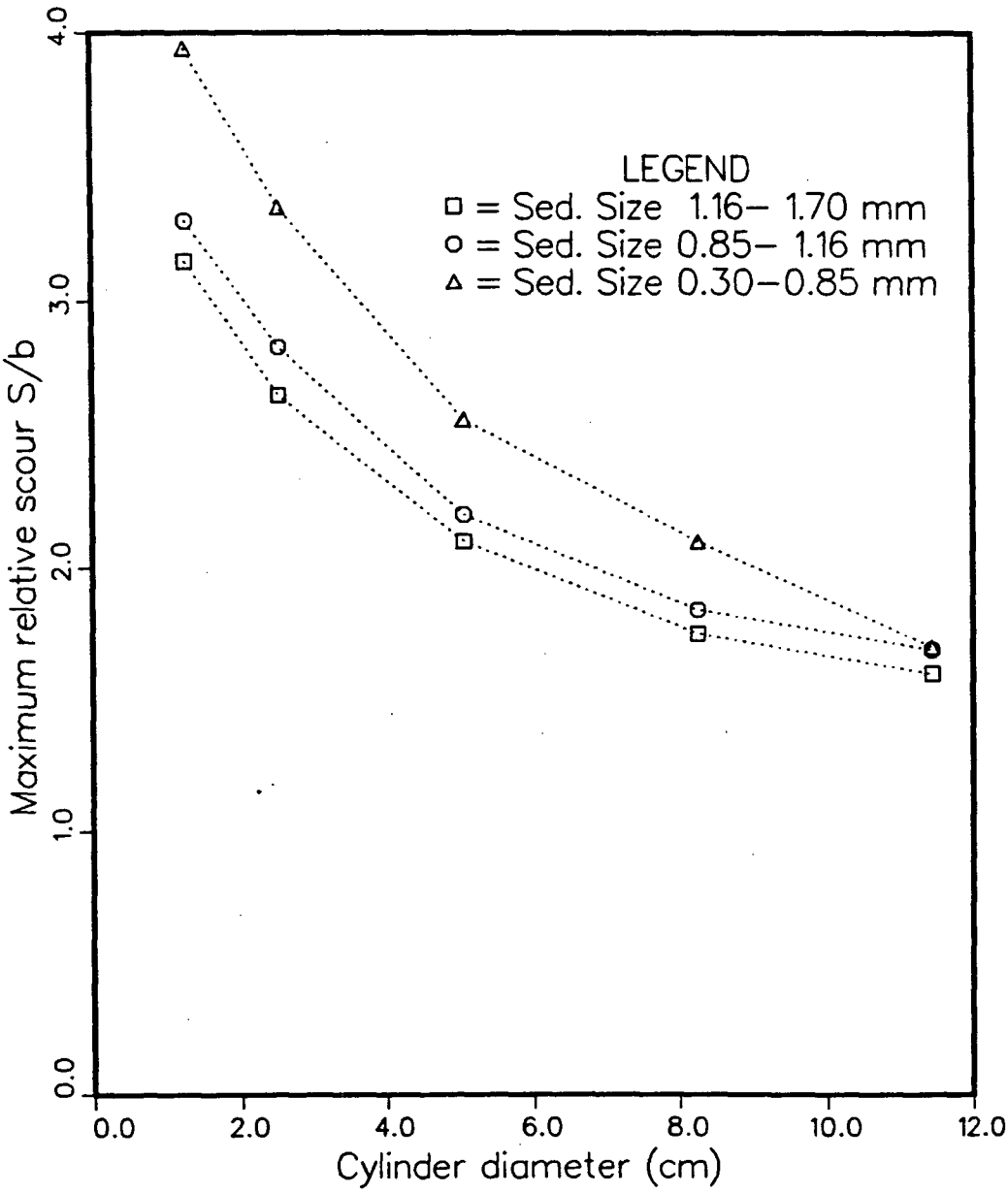

Figure 5.13. Maximum relative scour versus cylinder diameter for three sediment sizes at threshold of combined waves and currents; 25% wave and 75% current.

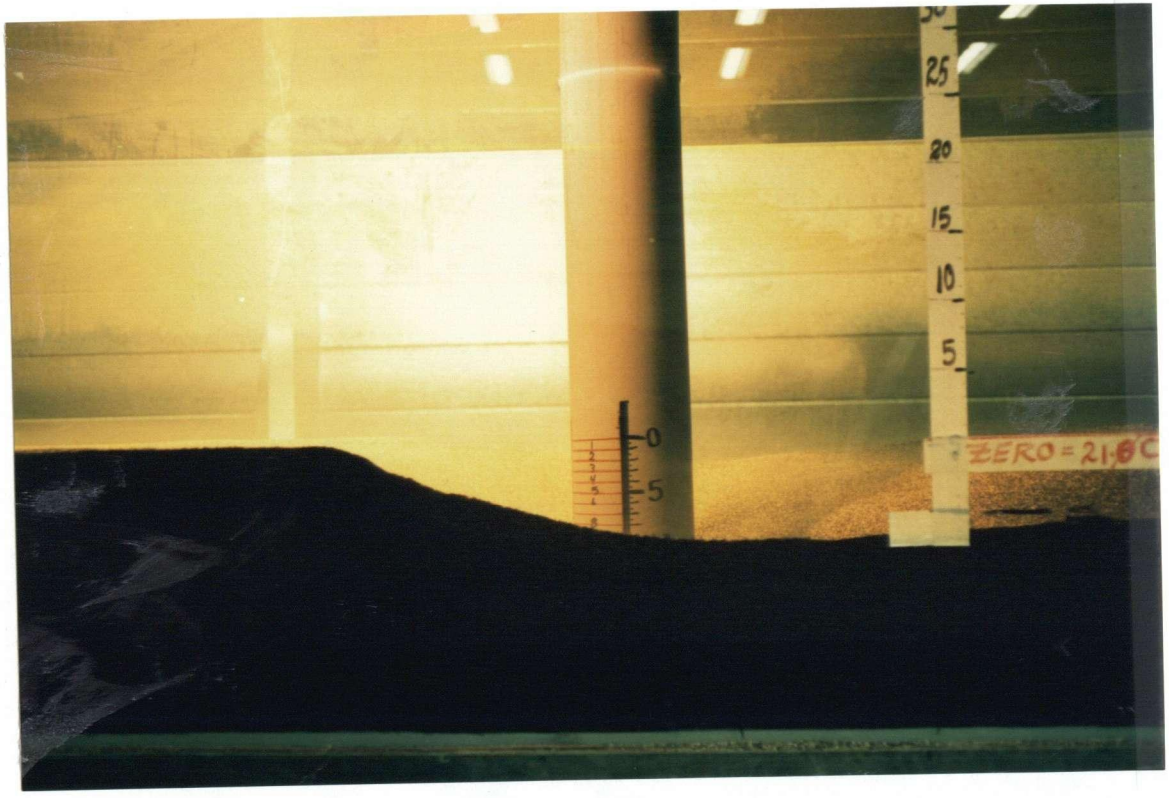

Figure 5.14. Typical scour hole pattern under combined waves and currents.

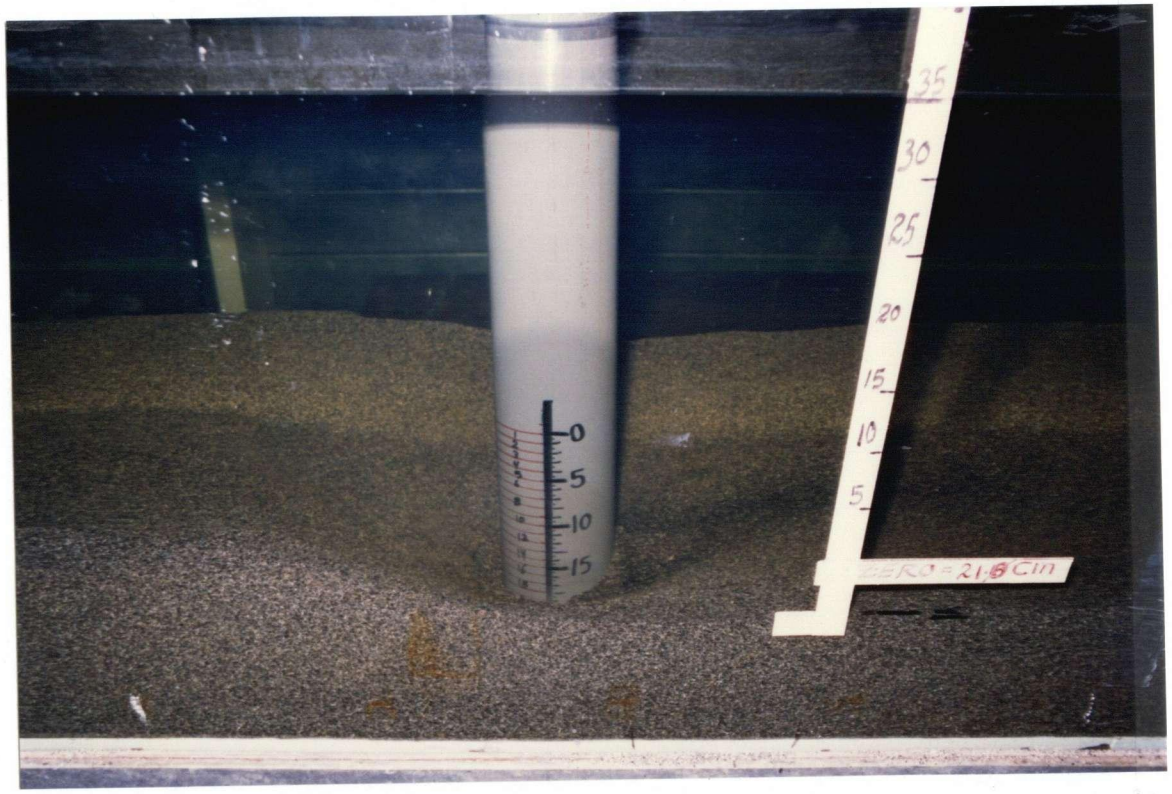

Figure 5.15. Typical scour hole pattern under combined waves and currents.

case of waves alone or waves plus currents, the sand bed might ripple as shown in Figures 5.16 and 5.17.

A comparison of the combined wave and current test results with results from other studies has not been possible, partly because of the lack of such a study, and partly because even with the few studies that are available, the comparison cannot be made because the problem was treated from another viewpoint. For example, previous studies investigated the dependence of scour on the flow parameters such as wavelength, wave height, water depth, etc., and at flow velocities less than the critical velocity. Also a single pile size and a single sediment size were utilized in these other studies. In the present study the emphasis was to determine the maximum possible scour, namely when the sandbed was at onset of motion, and this condition was studied using several pile and sediment sizes.

It is worthwhile to note that no distinct formulas for maximum scour prediction were reached due to the limited number of tests and limited studies in this field. However a rough estimate of the amount of maximum scour around cylindrical piles can be found using these study results. The bed material critical velocity for onset of motion can be known if the material properties are known, then the flow velocity at bed can be calculated provided that flow parameters are defined, hence the contribution of each flow component is determined. Knowing the structure size the maximum possible scour around the structure can be estimated using Figures 5.8 through 5.13.

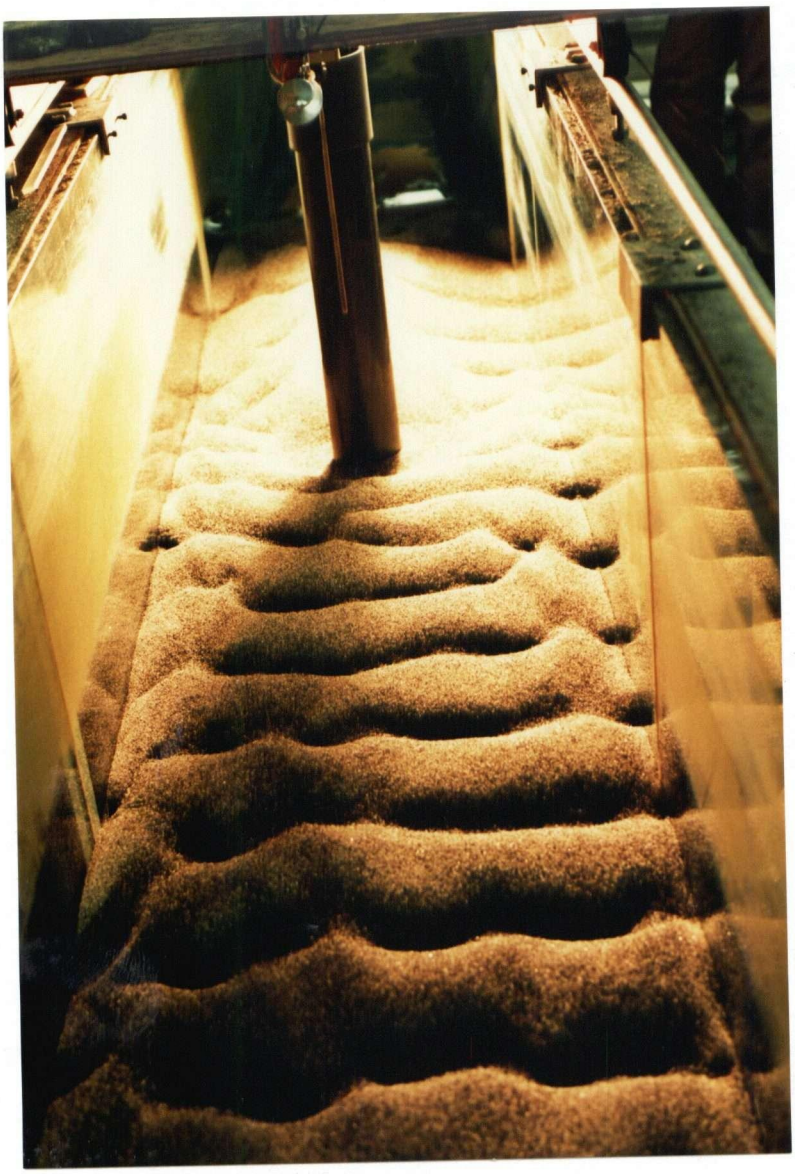

Figure 5.17. Typical ripple pattern under combined waves and currents.

Figure 5.16. Typical ripple-pattern under combined waves and currents.

6. CONCLUSIONS AND RECOMMENDATIONS

6.1 CONCLUSIONS

The purpose of this study is to compare the maximum possible scour around cylindrical piles under the action of combined waves and currents with the scour produced by pure waves and pure currents. The following conclusions were reached:

1. Scour around piles starts when the approach velocity is as low as 0.3-0.4 of the critical velocity. This is because the flow is accelerated by the pile.

2. The equilbrium scour conditions for pure currents are reached in less time than the equilibrium conditions for the combined waves and currents. However maximum scour under pure wave action is reached in much less time than for currents alone or waves and currents.

3. For all the cases tested the maximum possible scour was attained when approach flow conditions upstream of the pile reached the critical stress for onset of motion for sediment particles.

4. If threshold conditions are exceeded, i.e., the flow velocity is greater than the critical velocity for onset of motion, the equilibrium scour depth is less than the maximum scour depths under threshold conditions. The graphs of scour development as a function of time show that scour increases to a maximum and then decreases slightly as time increases. This decrease could possibly be caused by selective armouring of the scour hole with coarser material.

5. The development of combined wave and current scour with time is similar to that of unidirectional flow, except for the rate of development as noted in (2).

6. The pattern of scour hole is quite similar under the three flow cases tested.

7. For all the cases, the maximum scour depth was adjacent to the leading edge of the pile.

8. For the case of combined waves and currents at threshold conditions, the maximum scour is dependent on the relative contribution of both steady and unsteady components of flow to the threshold velocity of the sediment material. The higher the steady current percentage, the deeper is the scour hole, so that in the limit the pure current produces the deepest scour. On the other hand, the more the contribution of the wave, the less is the scour depth and in the limit of pure waves, the scour depth is minimum, provided that the same size of cylinder is used. Therefore, when considering maximum scour depth under combined waves and currents, it is necessary to know the amount of each flow component in the combined threshold velocity.

9. The scour depth under waves plus currents is more sensitive to the flow component contributions when the cylinder size is large than when the cylinder is small.

10. It was observed that the combined wave and current scour depth is only slightly dependent on sediment size, especially for bigger diameter piles. However, scour depths for small sediment size ranges are slightly greater than for bigger sediment size ranges.

11. The measured scour depths under currents alone were compared with estimated or calculated values using available scour prediction formula. The measured values are in a good agreement with most of the estimated values in specific formulas (1.7) and (1.8). Therefore steady flow estimates of scour provide an upper bound on the scour depth.

12. Knowing the flow parameters and the structure size and bed material properties, it is possible to get at least a rough estimate of the maximum possible scour.

6.2 RECOMMENDATIONS FOR FURTHER STUDY

There are several areas in which further studies could be made to improve the present study.

1. It would be desirable to repeat these experiments using different size sand ranges to evaluate the effect of sediment size more precisely.

2. Although this study was restricted to non-cohesive material, similar experiments can be run again using cohesive material.

3. Using larger pile sizes and conducting the same experiments in a larger flume could indicate the pile size dependence, and to find a certain correlation or formula for maximum scour.

4. Using an array of piles and varying the spacing could identify a spacing parameter indicating at what distance the piles must be separated in order for them to scour independently of one another.

5. Installation of a protective collar on piles and repeating the same experiments could identify the spacing and the size of these collars to reduce scour.

6. Throughout the experiments the wave used was uniform, two-dimensional of the sinusoidal type. This study could be extended to investigate the effect of random waves on scour depth around structures.

7. Other shapes of piles - rather than the cylindrical shape - could be tested.

BIBLIOGRAPHY

Abad, G.N. and Machemehi, J.L. (1974), "An Experimental Study of Scour Around Marine Foundations Due to Oscillatory Waves and Unidirectional Currents," Centre for Marine and Coastal Studies, North Carolina State University, Report No. 74-5.

Alger, G.R. and Simons, D.B. (1968), "Fall Velocity of Irregular Shaped Particles," Journal of the Hydraulics Division, ASCE, Vol. 94, No. HY3, pp. 721-737.

Anderson, A.G. (1974), "Scour at Bridge Waterways - A Review," Report No. FHWA-RD-75.89, Federal Highway Administration, Washington, D.C.

Armbrust, S.L. (1982), "Scour About Cylindrical Pile Due to Steady and Oscillatory Motion," M.S. Thesis, Texas A&M University, College Station, Texas.

Bagnold, R.A. (1946), "Motion of Waves in Shallow Water, Interaction Between Waves and Sand Bottoms," Proc. Roy. Soc. London, Series A, Vol. 187, pp. 1-18.

Bagnold, R.A. (1966), "An Approach to the Sediment Transport Problem From General Physics," U.S. Geological Survey Professional Paper No. 422-I, pp. I1-I37.

Bakker, W.T. (1974), "Sand Concentration in an Oscillatory Flow, Proceedings, 14th Conf. on Coastal Engineering, Copenhagen.

Bakker, W.T. and Van Doorn, Th. (1978), "Near Bottom Velocities in Waves With a Current," Proceedings, 16th Conf. on Coastal Engineering.

Bijker, E.W. (1967), "The Increase of Bed Shear in a Current Due to Wave Motion," Delft Hydraulics Laboratory, Publication No. 46, Delft, The Netherlands.

Breusers, H.N.C., Nicollete, G. and Shen, H.W. (1977), "Local Scour Around Cylindrical Piers," Journal of Hydraulic Research, International Association for Hydraulic Research, Vol. 15, No. 3.

Brevik, I. and Aas, B. (1980), "Flume Experiment on Waves and Currents. I. Rippled Beds," Coastal Engineering, 3, pp. 148-177.

Brevik, I. (1981), "Oscillatory Rough Turbulent Boundary Layers," Journal of Waterways, Port and Ocean Division, ASCE, Vol. 107, No. WW3, pp. 175-188.

Carstens, T. and Sharma, H.R. (1975), "Local Scour Around Large Obstruction," IHAR? Congress Vol. 2, pp. 251-262.

Chabert, J. and Engeldinger, P. (1956), "Etude des Affouillements autour des Piles de Ponts," Lab. d'Hydr. Chatou.

Coleman, N.L. (1967), "A Theoretical and Experimental Study of Drag and Lift Forces Acting on a Sphere on a Hydraulic Stream Bed," Proceedings, 12th Congress, IAHR, Vol. 3, Sec. C18, C19.

Eagleson, P.S., Dean, R.G. and Peralta, L.A. (1958), "The Mechanics of the Motion of Discrete Particles Due to Shoaling Waves," U.S. Army Corps of Engineers, Beach Erosion Board, Tech. Memo No. 104, 55p.

Eagleson, P.S. and Dean, R.G. (1961), "Wave Induced Motion of Bottom Sediment Particles," Transactions, ASCE, Vol. 126, Part 1, pp. 1162-1189.

Fenton, J.D. (1979), "A High-Order Cnoidal Wave Theory," JFM, Vol. 94, pp. 129-161.

Fredsoe, J. (1984), "Turbulent Boundary Layer in Wave-Current Motion," J. Hydr. Eng., ASCE, Vol. 110,1 No. 8, pp. 1103-1120.

Grant, W.D. and Madsen, O.S. (1979), "Combined Wave and Current Interaction With a Rough Bottom," J. Geophy. Res. 84, pp. 1797-1808.

Grass, A.J. (1970), "Initial Instability of Fine Bed Sand," J. Hydr. Div., ASCE, Vol. 96, No. HY3, pp. 619-632.

Hanco, S. (1971), "Sur le Calcul des Affouillements Locaux dans la Zone des Piles de Ponts," Proceedings, 14th IAHR Congress, Paris, 3, pp. 299-313.

Henderson, F.M. (1966), "Open Channel Flow," Ed. Gene Nordby, MacMillan Publishing Co., Inc., New York, 522p.

Herbich, J.B., Murphy, H.D. and Van Weels, B. (1965), "Scour of Flat Sand Beaches Due to Wave Action in Front of Seawalls," Proc., Coastal Engineering, Santa Barbara Specialty Conference, Chapter 28, pp. 703-726.

Hincu, S. (1965), "Cuprivire la Calculul a Fuierilor Locale in Zone a Pileor Podulil," Hidrotechnica, Gospodarirea a pelor, Meteorologia, 10(1), pp. 9-13.

Horikawa, K. and Watanabe, A. (1967), "A Study of Sand Movement Due to Wave Action," Coastal Engineering in Japan, Vol. 10, pp. 39-57.

Imberger, J., Alach, D. and Schepis, J. (1982), "Scour Behind Circular Cylinders in Deep Water," Coastal Eng. Proc., V. 2, pp. 1523-1527.

Jain, S.C. and Fisher, E. (1979), "Scour Around Bridge Piers at High Froude Numbers," Report No. FH-WA-RD-79-104, Federal Highway Administration, Washington, D.C.

Jain, S.C. and Fisher, E.E. (1980), "Scour Around Bridge Piers at High Flow Velocities," Proc. Am. Soc. Civil Eng., J. Hydraulic Division, Vol. 106, No. HY11, pp. 1828-1840.

Johnes, G.E. (1970), "Scour at Bridges Waterways," Highway Research Board, Division of Engineering, National Research Council, National Academy of Engineering.

Johnsson, I.G. (1966), "Wave Boundary Layers and Friction Factors," Proc. 10th Coastal Eng. Conf., Tokyo, Vol. I, pp. 127-148.

Kajiura, K. (1968), "A Model of the Bottom Boundary Layer in Water Waves," Bulletin of the Earthquake Research Institute, Vol. 46, pp. 75-123.

Kamphuis, J.W. (1975), "Friction Factor Under Oscillatory Waves," J. Waterways Harbors and Coastal Eng. Div., ASCE, Vol. 101, No. WW2, pp. 135-144.

Kemp, P.H. and Simons, R.R. (1982), "The Interaction Between Waves and a Turbulent Current: Waves Propagating With the Current," J. Fluid Mech., Vol. 116, pp. 227-250.

Kemp, P.H. and Simons, R.R. (1983), "The Interaction Between Waves and a Turbulent Current: Waves Propagating Against the Current," J. Fluid. Mech., Vol. 130, pp. 73-89.

Ko, S.C. (1967), "Scour of Flat Sand Beaches in Front of Seawalls," Fritze Engineering Laboratory, Report No. 273.5.

Komar, P.D. and Miller, M.C. (1973), "The Threshold of Sediment Motion Under Oscillatory Water Waves," Journal of the Sedimentary Petrology, Vol. 43, pp. 1101-1110.

Komar, P.D. and Miller, M.C. (1974), "Sediment Threshold Under Oscillatory Waves," Proc. 14th Coastal Engineering Conference, Copenhagen, Vol. II, pp. 756-775.

Larras, J. (1960), "Recherches Experimentales sur l'érosion au pied d'une Pile de Pont," C.R. Acad. Sciences, 251(3), pp. 330-331.

Larras, J. (1963), "Profordeurs Maximales d'érosion des Fonds Mobiles autor des Pile en riviére," Ann. Ponts et chaussées, 133(4), pp. 411-424.

Laursen, E.M. and Toch, A. (1956), "Scour Around Bridge Piers and Abutments," Bull. No. 4, Iowa Highway Res. Board.

Madsen, O.S. and Grant, W.D. (1975), "The Threshold of Sediment Movement Under Oscillatory Waves: A Discussion," Journal of the Sedimentary Petrology, Vol. 45, No. 2, pp. 360-361.

Madsen, O.S. and Grant, W.D. (1976), "Quantitative Description of Sediment Transport by Waves," Proceedings of the 15th Coastal Engineering Conference, Honolulu, Vol. II, pp. 1093-1112.

Manohar, M. (1955), "Mechanics of Bottom Sediment Movement Due to Wave Action," U.S. Army Corps of Engineers, Beach Erosion Board, Tech. Memo No. 75, 121p.

Melville, B.W. (1975), "Local Scour at Bridge Sites," Report No. 117, University of Auckland, School of Engineering, Auckland, New Zealand.

Morison, J.R., O'Brien, M.B., Johnson, J.W. and Schaaf, S.A. (1950), "The Force Exerted by Surface Wave on Piles," Petrol. Trans., AIME, Vol. 189, pp. 149-154.

Murphy, M.D. (1964), "Scour of Flat Sand Beaches Due to Wave Action," Fritze Engineering Laboratory Report No. 293.3.

Neill, C.R. (1964a), "Local Scour Around Bridge Piers," Highway and River Engineering Division, Research Council of Alberta, Alberta, Canada.

Neill, C.R. (1964b), "River Bed Scour, A Review for Bridge Engineers," Res. Council of Alberta, Cont. No. 281, Calso Techn. Publ. No. 23, Canadian Good Roads Assoc., reprinted (1970).

Poscey, C.J. (1949), "Why Bridges Fail in Floods," Civil Engineers, 19, pp. 42-90.

Posey, C.J. (1971), "Protection of Offshore Structures Against Under Scour," Journal of the Hydraulics Division, ASCE, Vol. 97, No. HY7, pp. 1011-1016.

Quick, M.C. (1983), "Sediment Transport by Waves and Currents," Canadian Journal of Civil Engineering, Vol. 10, No. 1, pp. 142-149.

Quick, M.C., Kingston, K.W. and Lei, S. (1985), "Onset of Sediment Motion Under Waves and Currents," Can. Soc. Civ. Eng., Proc. 7th Can. Hydrotech. Conference, Saskatoon, Saskatchewan, pp. 107-125.

Rance, P.J. and Warren, N.F. (1969), "The Threshold Movement of Coarse Material in Oscillatory Flow," Proc. 11th Coastal Eng. Conf., London, Vol. I, pp. 487-491.

Roper, A.T., Schneider, V.R. and Shen, H.W. (1967), "Analytical Approach to Local Scour," Proc. 12th IAHR Congress, Ft. Collins, 3, pp. 151-161.

Sarpkaya, T. and Isaacson, M. de St. Q. (1981), "Mechanics of Wave Forces on Offshore Structures," Van Nostrand Reinhold Company, New York.

Shen, H.W. (1971), "River Mechanics," Vol. 2, Chapter 23, Scour Near Piles; Ft. Collins.

Shen, H.W., Schneider, V.R. and Karaki, S. (1966a), "Mechanics of Local Scour," Colorado State Univ., CER66, HWS-VRS-SK22.

Shen, H.W., Schneider, V.R. and Karaki, S. (1969), "Local Scour and Bridge Piers," J. of the Hydraulic Division, ASLE, Vol. 75, No. H46, pp. 1919-1940.

Shields, A. (1936), "Anwendung der Aehnlichkeitsmechanik und der Turbulenzforschung auf die Geshiebebewegung," Mitteilungen der Preuss. Versuchsanst fur Wasserbau und Schiffbau, Berlin, No. 26. Available also in a trnslation by W.P. Ott and J.C. van Uchelen, S.C.S. Cooperative Laboratory, California Institute of Technology, Pasadena, California, as "Application of Similarity Principles and Turbulence Research to Bed-Load Movements".

Tanaka, H. and Shuto, N. (1984), "Friction Laws and Flow Regimes Under Wave and Current Motion," Journal of Hydraulic Research, Vol. 22, No. 4, pp. 245-261.

Vanoni, V.A., Benedict, P.C., Bondurant, D.C., McKee, J.E., (1966), "Sediment Transportation Mechanism: Initiation of Motion," Progress Report of the Task Committee on Preparation of Sedimentation Manual, Committee on Sedimentation, Journal of the Hydraulics Division, ASCE, Vol. 92, No. HY2, Proc. paper 4738.

Van Weels, B. (1965), "Beach Scour Due to Wave Action on Seawalls," Fritze Engineering Laboratory Report No. 293.3.

Wang, R.K. and Herbich, J.B. (1983), "Combined Current and Wave Produced Scour Around a Single Pile," Texas Engineering Experiment Station, Report No. COE269, Texas A&M University, College Station, Texas.

Wells, D.R. and Sorensen, R.M. (1970), "Scour Around a Circular Pile Due to Oscillatory Wave Motion," Sea Grant Publication No. 208, COE Report, No. 113, Texas A&M University.

White, C.M. (1940), "The Equilibrium of Grains on the Bed of a Stream," Proceedings of the Royal Society (A), Vol. 174, pp. 322-338.

Williams, P.B. and Kemp, P.H. (1971), "Initiation of Ripples on Flat Sediment Beds," J. Hydr. Div. ASCE, Vol. 97, No. HY4, pp. 505-522.